International Journal of Heat and Mass Transfer 186 (2022) 122457

Contents lists available at ScienceDirect

International Journal of Heat and Mass Transfer

journal homepage: www.elsevier.com/locate/hmt

Modelling hydraulic conductivity for porous building materials based on a prediction of capillary conductivity at capillary saturation

Jon Ivar Knarud[a,*], Tore Kvande[a], Stig Geving[b]

[a] Department of Civil and Environmental Engineering, Norwegian University of Science and Technology, NO-7491 Trondheim, Norway
[b] Department of Architecture, Materials and Structures, SINTEF Community, NO-7465 Trondheim, Norway

ARTICLE INFO

Article history:
Received 23 October 2021
Revised 10 December 2021
Accepted 19 December 2021

Keywords:
Liquid conductivity
Moisture diffusion
Thin film surface diffusion
Capillary absorption coefficient

ABSTRACT

Liquid moisture transport plays a key role in performance of many building assemblies. For hygrothermal simulation models, used to assess such assemblies, it is important to include realistic liquid transport properties for the specific porous building materials involved. Unfortunately, comprehensive experimental and modeling methods associated with determining the hydraulic conductivity limit widespread application of material-specific determination. To ease applicability, this paper investigates how to simplify conductivity prediction and modeling by building on a bundle of tubes approach. Incorporating a new expression variant for the capillary absorption coefficient (A_w), a novel prediction expression for the conductivity at capillary saturation ($K_{c,cap}$) is derived. modeling of unsaturated capillary conductivity (K_c) can thus be scaled to $K_{c,cap}$ instead of the traditional approach of scaling to conductivity at over-capillary saturation (K_{sat}), avoiding some complexity and concerns one traditionally has faced. Hence, in contrast to most models for K_c, which apply K_{sat}, this paper applies $K_{c,cap}$ as reference to scale the conductivity at unsaturated conditions. To model the hydraulic conductivity (K) for the full moisture range, K_c is coupled with a thin film model (K_{film}) and a hygroscopic correction model (K_{hyg}). The prediction model is evaluated against a wide range of porous building material datasets found in literature as well as compared to a common alternative approach, with reasonable results. The findings of this study can help for better understanding of challenges in analytical calculation of A_w and of why bundle of tube models have accuracy issues in predicting K_c, with the study suggesting remedies for some of these issues.

1. Introduction

Hygrothermal simulation has become an important tool for assessing the hygrothermal performance of building details or parts, either it concerns new designs or retrofits, renovations or improvements to existing buildings. When involving capillary moisture transport, it is important that capillary properties of porous materials are realistically captured. Of key interest is the moisture retention curve and the hydraulic conductivity curve. Of these the latter is the most challenging, as it is difficult to experimentally determine in the unsaturated region [1], and relatively resource intensive to determine (accurately) in the saturated region. Usually, one of two approaches are used to identify the hydraulic conductivity for the full range of moisture contents: 1) modeling which usually include scaling to the saturated conductivity, or 2) calculation from the moisture diffusivity. Although the moisture diffusivity is relatively easier to determine over unsaturated capillary conditions it is still resource intensive, traditionally involving experimentally determining moisture profiles and for instance applying the Boltzmann transform method to determine the moisture diffusivity function, e.g. [2]. Thus, for practical applications it is not obvious that the diffusivity approach is realistic to utilize [1]. Regarding modeling, hydraulic conductivity has often been modeled by bundle of tubes models, with the most well-known model contributions, originally developed for petroleum and soil science, being Burdine [3], Mualem [4] and Van Genuchten [5]. An alternative to bundle of tubes models have been the more advanced network models, which incorporate percolation theory [6, 7].

Although bundle of tubes models are not without flaws, with their oversimplification of the pore system and flow paths (e.g. [6]), their relative simplicity provides an approach less laborious and easier accessible to utilize than their network model alternatives [7]. Bundle of tubes models are commonly scaled from measured capillary conductivity at saturation K_{sat} or at zero capillary pressure K_0; however, these have shown to be difficult to determine accurately [8]. Furthermore, it has been reported difficulty

* Corresponding author.
E-mail address: jon.knarud@ntnu.no (J.I. Knarud).

https://doi.org/10.1016/j.ijheatmasstransfer.2021.122457

Nomenclature (excluding Table 1)

A	area (m^2)
$A_{int,v}$	cross sectional area of internal voids per unit area (m^2/m^2)
A_w	capillary absorption coefficient ($kg/(m^2\ s^{1/2})$)
B_A, B_c, B_f	area, curvature and flow rate correction factors due to pore shape irregularity (-)
$C_{int,v}$	circumference of internal voids per unit area (m/m^2)
D_w	diffusion coefficient (m^2/s)
$f_{curvature}$	film curvature correction factor (-)
f_d	factor of deviation (-)
f_l	mechanistic scaling function (-)
j	moisture flux ($kg/(m^2\ s)$)
K	hydraulic conductivity (kg/(m s Pa))
L	length (m)
l_w, c_w, n_w	coefficients for retention curve expression, (-), (Pa^{-1}), (-) respectively
m	mass (kg)
m''	mass uptake per unit area (kg/m^2)
$\dot{m}''$	mass rate per unit area ($kg/(m^2\ s)$)
n	cumulative pore number (-)
p	pressure (Pa)
r	capillary pore radius (m)
r_0, r_{eff}, r_{ae}	average, effective and average/effective pore radius (m)
R_w	gas constant for water (J/(kg K))
S_{wi}, S_{wf}	wetting phase saturation, initial and behind imbibition front respectively (-)
t	time (s)
T	temperature (K)
V	volume (m^3)
$\dot{V}$	volumetric flow rate (m^3/s)
$\dot{V}'$	volumetric flow rate per unit length ($m^3/(m\ s)$)
V''	absorbed volume per unit area (m^3/m^2)
w	moisture content (kg/m^3)
x	spatial coordinate (m)

Greek symbols

α	correction factor (-)
α_p	dimensionless pressure (-)
δ	film thickness (m)
δ_v	vapor diffusion coefficient (kg/(m s Pa))
ε	porosity (-)
η_{Aw}, η_{cap}	various scaling factors (-)
η_{sp}, η_ϕ	various exponents (-)
θ	moisture content (m^3/m^3)
μ	vapor diffusion resistance (-)
μ_w	dynamic viscosity water (kg/(m s))
Π, Π_e, Π_m,	disjoining pressure, with electrostatic and molecular components (Pa)
ρ_w	density water (kg/m^3)
σ_w	surface tension water (N/m)
τ	tortuosity (-)
φ	contact angle (°)
ϕ	relative humidity (%)

Subscripts

a	air
abs	absorption
ad	adsorbed
c	capillary
cap	capillary saturation
dry	dry cup measurement
Dw	diffusion coefficient based
eff	effective
film	adsorbed moisture film
g	gas
hyg	hygroscopic
l	liquid
lim	limiting
mod	modified
nom	nominal
p	pore
red	redistribution
ref	reference
rel	relative
sat	saturation
tot	total
v	vapor
w	water
wet	wet cup measurement

with scaling to the saturated conductivity, when saturation is set equal to total porosity, because the moisture retention curve is ill-defined in the over capillary region close to saturation [9].

Nevertheless, to accommodate an engineering need for less resource intensive predictions of hydraulic conductivity, bundle of tubes models are still of interest. With a bundle of tubes model as the foundation, Scheffler and Plagge [7] proposed a whole moisture range hydraulic conductivity model. Although this model is intriguing, it relies on a couple of material dependent parameters which require iterative post-processing through simulation to be determined properly. Furthermore, the model still relies on scaling to an effective conductivity at over-capillary saturation, which needs to be determined experimentally. Equipment for, and experience with, such experimental determination is not particularly available for wide practical application.

In the present paper the aim has been to develop a model, inspired by the Scheffler and Plagge model, but which is easier to apply, by removing reliance on iterative post-processing and reducing reliance on material property data which is particularly resource intensive to acquire.

Specifically, the objective of this study is to derive and investigate an alternative approach to predict hydraulic conductivity as function of capillary pressure, $K(p_c)$, not relying on comprehensive testing of K (or K_{sat}) in contrast to existing approaches.

From initial, inspirational ideas research questions were formulated to substantiate the objective. The following questions are explored in our study: 1) Is it feasible to predict the capillary conductivity at capillary saturation? 2) Can the Scheffler-Plagge model for $K(p_c)$ be simplified by scaling to conductivity at capillary saturation instead of at saturation? 3) Can the overall procedure for determining $K(p_c)$ be simplified and made more practically feasible, for when only a necessary minimum of material property test data is available. 4) For such a model, how is the prediction performance for $K(p_c)$ when assessing a wide range of porous building materials described in previous studies?

The focus of this paper is categorically limited to bundle of tubes models, in description of the hydraulic conductivity, in contrast to network models. Hysteresis effects are not addressed. Furthermore, needed information on the pore size distribution will be estimated from the retention curve, and it has been outside the scope of the work to assess whether direct use of a measured pore size distribution would improve predictions. The study does not include a comparative evaluation of how realistic physics are represented in comparable, alternative prediction approaches; however,

a quantitative comparative evaluation of prediction performance is included.

The paper is outlined as follows: First the model is derived and presented. Then procedure for its application and evaluation is introduced. After follows results and result assessments, followed by further discussion and finally a summary and conclusion.

2. Hydraulic conductivity model

Several hydraulic conductivity models for the whole moisture range have previously been proposed, e.g., within field of building physics [7, 10] and soil science [11, 12]. In contrast to the former the latter include models for thin film flow to the overall hydraulic conductivity. With thin film flow models seemingly having benefitted conductivity modeling at low moisture contents in soil science, it is possible similar benefits can be introduced to application in building physics. Thin film flow will therefore be incorporated in the overall hydraulic model presented in the following sections. In this study we will limit the hydraulic conductivity model to liquid conductivity, with the presumption that vapor transport is addressed separately in hygrothermal simulation software. Hence, vapor transport (vapor conductivity) is not included.

In the following sections we go through the sequential steps of deriving the hydraulic conductivity model. First we introduce the bundle of tube model based on Grunewald et al. [10]. Then theory on predicting the capillary absorption coefficient is introduced followed by a proposed new prediction expression. Next, this enables forming a prediction expression for the capillary conductivity at capillary saturation. Further, the Sceffler and Plagge model [7] is rearranged for scaling to conductivity at capillary saturation. Thereafter follows a thin film model based on Lebeau and Konrad [11] and a correction model for the hygroscopic region based on the Sceffler and Plagge model [7]. The overall hydraulic model is then established. Finally, a procedure for incorporating the retention curve into the model is given.

2.1. Capillary conductivity

The Hagen-Poiseuille equation describes the volumetric laminar flow in a cylindrical pore (tube) of radius r along the tube path of length L. However, pores in porous media usually never meet the ideal of cylindrical geometry [13]. Therefore, a flow rate correction factor B_f is included to account for impact of irregular geometry (non-cylindrical), on the volumetric flow rate. In contrast to Cai et al. [13], which relates a correction factor α directly to r, B_f is here related to the volumetric flow rate; hence, B_f equates to α^4 in [13]. The Hagen-Poiseuille equation thus take the form:

$$\dot{V}(r) = -B_f \frac{\pi r^4}{8\mu_w} \frac{dp_l}{dL} \tag{1}$$

where μ_w is the dynamic viscosity of water and p_l the liquid pressure. With capillary pressure $p_c = p_g - p_l$ and presumed constant gas (air) pressure p_g, dp_l is simply substituted with $-dp_c$. Here, for convenience, positive values for p_c are applied throughout, although p_c alternatively can be written as negative pressure (suction). r represents an equivalent cylindric radius, in practical terms, half of a hydraulic diameter, or the radius of an inscribed circle for regular polygons. Flow in capillaries may be perceived to follow tortuous streamlines [13, 14]. Consequently, the flow path length dL is greater than a more relatable dimension dx, of a control volume. This can be addressed by introducing the tortuosity τ, which from a macroscopic perspective represents the ratio of effective capillary path length to length dx (thickness of a control volume). That is; $dL = \tau \bullet dx$, see e.g. [15]. With these changes, Eq. (1) transforms to:

$$\dot{V}(r) = B_f \frac{\pi r^4}{8\mu_w} \frac{1}{\tau} \frac{dp_c}{dx} \tag{2}$$

The volumetric flow rate in a bundle of capillaries can be found by integrating Eq. (2) over the pore size distribution density [7, 10], i.e. integrating with respect to radius the product of volumetric flow rate and corresponding incremental number of pores at respective radius. Adapted from [7, 10] the capillary moisture flux then becomes:

$$j_{w,x} = \rho_w \int_R \dot{V}(r) \frac{dn(r)}{dr \cdot dA} dr \tag{3}$$

where j_w is the moisture flux, and dA indicates unit area $dA = dydz$ of a control volume $dV = dxdydz = 1\ \mathrm{m}^3$.

The expression for the incremental number of pores can be established as follows:

$$dn(r) = \frac{\Delta V(r)}{A_p(r)\tau dx} = \frac{\Delta\theta_c \cdot dV}{B_A \pi r^2 \tau dx} = \frac{dA}{B_A \pi r^2 \tau} \frac{d\theta_c(r)}{dr} dr \tag{4}$$

where $dn(r)$ is the increment number of pores at a radius, $\Delta V(r)$ change in moisture filled capillary volume as function of r, $A_p(r)$ pore cross section, θ_c volumetric capillary retained moisture content. B_A area correction factor for non-circular cross section $B_A = A_p/A_{p,cylindrical}$ (e.g. $B_A = 1.27$ square, $B_A = 1.65$ equilateral triangle). Including the factor B_A is important to account for the "extra" water in each pore which is not included in the inscribed circle which r represents. For non-circular cross sections, not including B_A will overestimate the number of pores. Rearranging Eq. (4) we have:

$$\frac{dn(r)}{dr \cdot dA} = \frac{1}{B_A \pi r^2 \tau} \frac{d\theta_c(r)}{dr} \tag{5}$$

Note that by including B_A and τ, Eqs. (4) and (5) differs from the approach in [7, 10]. Inserting Eqs. (2) and (5) into Eq. (3) and integrating over all radii involved at a capillary moisture content θ_c:

$$j_{w,x} = \frac{B_f}{B_A} \frac{\rho_w}{8\mu_w \tau^2} \int_0^{\theta_c} r(\theta_c)^2 d\theta_c \frac{dp_c}{dx} \tag{6}$$

Eq. (6) is similar to what is reported in [7], but with the additional inclusion of tortuosity and the factors B_f and B_A. The radius can be related to the capillary pressure through the Young-Laplace equation, which when given by Eq. (7) includes a correction factor B_c for pore shape irregularity [13, 16]. This irregularity affects the meniscus curvature, see [17].

$$p_c = \frac{2\sigma_w \cos(\varphi)}{r/B_c} \tag{7}$$

where σ_w is the surface tension of water and φ the contact angle. Following Wong et al. [17] the general Young-Laplace equation can be arranged:

$$p_c = \frac{\sigma}{r} \nabla \cdot \hat{\boldsymbol{n}} \rightarrow \frac{r p_c}{\sigma} \equiv \alpha_p = \nabla \cdot \hat{\boldsymbol{n}} \tag{8}$$

where α_p is a dimensionless pressure and $\nabla \bullet \hat{\boldsymbol{n}}$ is the dimensionless mean curvature.

B_c can then be defined as:

$$B_c = \frac{\alpha_{p,actual}}{\alpha_{p,cylindrical}} \tag{9}$$

Considering Eqs. (8) to (7), $\alpha_p = 2cos(\varphi)$ for a cylindrical pore. Assuming 0° contact angle; for a cylindrical pore $\alpha_p = 2$ (Eq. (9): $B_c = 1.0$), for an equilateral triangle shaped pore $\alpha_p = 1.7776$ [17, 18] ($B_c = 0.8888$), and for a square shaped pore $\alpha_p = 1.8862$ [17, 18] ($B_c = 0.9431$). Note that the correction factor assigned by Cai et al. [13] as α, would here equate to $\alpha = B_f^{1/4} = 1/B_c$. For an equilateral triangle $\alpha = 1.186$ and a square $\alpha = 1.094$ [13] (α can

be found from assessing calculated analytical solutions of Hagen-Poiseuille flow for respective pore shapes). These α-values coincide with $\alpha = B_f^{1/4} \neq 1/B_c$. Thus, in [13] the two correction factors, respectively for the Hagen-Poiseuille and Young-Laplace equation, are incorrectly conflated into one and the same.

Inserting Eq. (7) solved for r into Eq. (6) gives:

$$j_{w,x} = \frac{B_f B_c^2}{B_A} \frac{\rho_w \sigma_w^2 \cos^2(\varphi)}{2\mu_w \tau^2} \int_0^{\theta_c} \frac{1}{p_c(\theta_c)^2} d\theta_c \frac{dp_c}{dx} \tag{10}$$

with the capillary conductivity in Eq. (10) being:

$$K_c = \frac{B_f B_c^2}{B_A} \frac{\rho_w \sigma_w^2 \cos^2(\varphi)}{2\mu_w \tau^2} \int_0^{\theta_c} \frac{1}{p_c(\theta_c)^2} d\theta_c \tag{11}$$

K_c becomes $K_{c,cap}$, i.e. capillary conductivity at capillary saturation, when integrated up to $\theta_c = \theta_{c,cap}$, By including pore shape correction factors and tortuosity Eq. (11) distinctly differs traditional approaches. Although, it is not particularly useful since B_f, B_c and B_A are still unknown factors. However, $K_{c,cap}$ has previously been suggested to be predicted from the capillary absorption coefficient A_w [19], as $K_{c,cap} = 10^{-8} \eta_{Aw} A_w^2$, where η_{Aw} being a material dependent coefficient reported to be in the interval 0.95 – 16.0. This expression is neither specifically sophisticated in its intuitiveness (non-correct or hidden units) nor convincingly related to physical characteristics of the material and fluid. Furthermore, with a coefficient spanning over one order of magnitude prediction accuracy suffers without experience in choosing the coefficient.

Nevertheless, if assuming $K_{c,cap}$ could be predicted from A_w, a dimensional analysis of K through the Rayleigh method [20] reveals that an expression of K could be a function of A_w^2 divided by a density characteristic, units [kg/m^3], and a pressure characteristic, unit [Pa]. (This does not necessarily exclude other possibilities of physical parameters.) Guessing the correct appearance however would not necessarily be straight forward, risking becoming heavily reliant on a nonsensical coefficient. A plausible approach is to presume more information is needed regarding A_w to understand the relation to K.

2.2. Capillary absorption coefficient

An expression for A_w was derived by Beltran et al. [21] to be:

$$A_w = \rho_w \left(\frac{\sigma_w}{\mu_w}\right)^{1/2} \frac{\varepsilon_{cap}}{\tau} r_0^{1/2} \left(\frac{\cos\varphi}{2}\right)^{1/2} \tag{12}$$

where ε_{cap} is the capillary porosity and r_0 is an average pore radius. Eq. (12) can also be directly derived from the early Handy imbibition model [13, 22], with the liquid permeability $k_w = \varepsilon_{cap} r_0^2/(8\tau)$ [21, 23]. As seen, Eq. (12) does not include correction for pore shape irregularity; however a similar expression by Benavente et al. [24], has one such correction included.

$$A_w = B_c^{1/2} \rho_w \left(\frac{\sigma_w}{\mu_w}\right)^{1/2} \frac{\varepsilon}{\tau^{1/2}} r_{eff}^{1/2} \left(\frac{\cos\varphi}{2}\right)^{1/2} \tag{13}$$

where ε is the porosity and r_{eff} is an effective radius which requires to be calculated by Newton's iteration method, see [24]. Hypothetically, with measurement of A_w one can thereby estimate B_c. Unfortunately, Eq. (13) suffers from some shortcomings, including; incorrect handling of the tortuosity, not including a correction factor in the Hagen-Poiseuille equation and not addressing the wetting liquid saturation [13]. A further developed expression can be found from an imbibition model derived by Cai et al. [13]:

$$A_w = \alpha^{3/2} \rho_w \left(\frac{\sigma_w}{\mu_w}\right)^{1/2} \frac{\varepsilon \left(S_{wf} - S_{wi}\right)}{\tau} r_{ae}^{1/2} \left(\frac{\cos\varphi}{2}\right)^{1/2} \tag{14}$$

where S_{wf} is the wetting phase saturation behind the imbibition front, S_{wi} the initial wetting phase saturation, and r_{ae} an average/effective pore radius. If assuming S_{wf} equals capillary saturation and S_{wi} is negligible, i.e. for an initially dry material or for a relatively non-hygroscopic material, then $\varepsilon(S_{wf} - S_{wi}) \approx \varepsilon_{cap}$. Even though Eq. (14) is a considerable improvement from Eq. (12) it also has its issues. As previously mentioned, the correction factors for the Hagen-Poiseuille and Young-Laplace equations have incorrectly been conflated in α. Furthermore, for materials having a pore structure of highly varying pore size it is difficult to assess r_{ae}.

Thereby, to accommodate these issues a revised derivation approach to A_w is warranted.

2.3. Proposed new A_w-expression

In the following an expression for A_w is derived with derivation steps from Cai et al. [13] coupled with approaches from Section 2.1.

Specifically addressing imbibition where a face of a porous material is put in contact with a free water surface, and assuming sharp-front theory of capillary absorption [25], there will be a sharp moisture front which moves through the material. We furthermore assume dealing with materials and a setting which follow linear cumulative absorption with respect to square root of time, i.e., $m'' = A_w\sqrt{t}$, where m'' is cumulative liquid mass absorption per unit area. Proportionality to $\sqrt{t}$ corresponds to a specific time-dependent imbibition regime in which neither inertia nor gravitational forces are significant. A thorough review of the imbibition regimes is provided by Dejam et al. [26].

In Eq. (1) dp_l is replaced with $-dp_c$ as before, but with dL now the distance L (pore length) the imbibition moisture front has traveled. Similar to [13], p_c is furthermore replaced with Eq. (7). Consequently, the volumetric flow rate of one pore can be expressed as:

$$\frac{dV_p}{dt} = B_f B_c \frac{\pi r^3}{4\mu_w} \frac{\sigma_w \cos(\varphi)}{L} \tag{15}$$

Assuming Eq. (15) only addresses capillary pores, initially being dry, which through the imbibition process becoming fully saturated between the free liquid surface and the moisture front, we have $V_p = L \bullet A_p$. Substituting L in Eq. (15) with V_p/A_p enables Eq. (15) to be integrated with regard to V_p and t. Integrating limits are; for $t = 0$, $V_p = 0$, and for $t = t$, $V_p = V_p$. Hence:

$$\frac{1}{2} V_p^2 = B_f B_c \frac{\pi r^3}{4\mu_w} \sigma_w \cos(\varphi) A_p t \tag{16}$$

The absorbed volume of water V_p can be integrated over the bundle of capillaries involved by repeating the same approach as in Eq. (3). Solving Eq. (16) for V_p and integrating over the pore size distribution density:

$$V'' = \int_R \left[B_f B_c B_A \frac{\pi^2 r^5}{2\mu_w} \sigma_w \cos(\varphi) t \right]^{1/2} \frac{dn(r)}{dr \cdot dA} dr \tag{17}$$

Applying Eq. (5), Eq. (17) becomes:

$$V'' = \int_0^{\theta_{c,cap}} \left[\frac{B_f B_c}{B_A} \frac{r}{2\mu_w} \sigma_w \cos(\varphi) t \right]^{1/2} \frac{1}{\tau} d\theta_c \tag{18}$$

Multiplying Eq. (18) with the water density, and rearranging:

$$m'' = \frac{B_f^{1/2} B_c^{1/2}}{B_A^{1/2}} \rho_w \left(\frac{\sigma_w}{\mu_w}\right)^{1/2} \left(\frac{\cos\varphi}{2}\right)^{1/2} \frac{1}{\tau} \int_0^{\theta_{c,cap}} r^{1/2} d\theta_c \cdot t^{1/2} \tag{19}$$

From Eq. (19) it follows that:

$$A_w = \frac{B_f^{1/2} B_c^{1/2}}{B_A^{1/2}} \rho_w \left(\frac{\sigma_w}{\mu_w}\right)^{1/2} \frac{1}{\tau} \int_0^{\theta_{c,cap}} r^{1/2} d\theta_c \left(\frac{\cos\varphi}{2}\right)^{1/2} \tag{20}$$

Comparing Eqs. (20) to (14) one can see $\alpha^{3/2}$ is recovered if one allows the incorrect conflation $\alpha = B_f^{1/4} = 1/B_c$ previously addressed. In derivation of Eq. (20) it is assumed $\varepsilon S_{wf} = \varepsilon_{cap} = \theta_{c,cap}$,

and S_{wi} is through the integral step to Eq. (16) implicitly assumed to be negligible ($S_{wi} = 0$). Both can be included by multiplying Eqs. (17)-(20) with $\varepsilon(S_{wf} - S_{wi})/\varepsilon_{cap}$. Nevertheless, the biggest difference to Eq. (14) is the treatment of the pore structure, in Eq. (20) with the integral of pore radii involved in capillary absorption over the interval of saturation up to capillary saturated moisture content $\theta_{c,cap}$.

Replacing r by means of the Young-Laplace equation, Eq. (7), Eq. (20) finally becomes:

$$A_w = \frac{B_f^{1/2} B_c}{B_A^{1/2}} \frac{\rho_w \sigma_w}{\mu_w^{1/2}} \frac{\cos(\varphi)}{\tau} \int_0^{\theta_{c,cap}} \frac{1}{p_c^{1/2}} d\theta_c \tag{21}$$

2.4. Proposed novel prediction of conductivity at capillary saturation

Taking the square of Eq. (21), solving for the unknown correction factor product $B_f B_c{}^2 B_A{}^{-1}$ and inserting into Eq. (11), $K_{c,cap}$ can finally be predicted by:

$$K_{c,cap} = \frac{A_w^2}{2\rho_w} \int_0^{\theta_{c,cap}} \frac{1}{p_c^2} d\theta \left[\int_0^{\theta_{c,cap}} \frac{1}{p_c^{1/2}} d\theta_c \right]^{-2} \tag{22}$$

Eq. (22) satisfies the dimensional analysis previously mentioned with the density characteristic revealed to be the density of water and the pressure characteristic expressed as a relation of two integrals both of functions of p_c.

2.5. Capillary model

With $K_{c,cap}$ being the capillary conductivity at capillary saturation the capillary model for saturations $0 \le \theta_c \le \theta_{c,cap}$ can follow the capillary model of Scheffler and Plagge [7]; $K_c = f_l \eta_{cap} K_{eff,sat} K_{rel}$, in where $f_l(w_{cap})\eta_{cap} K_{eff,sat}$ equals $K_{c,cap}$. η_{cap} is a scaling parameter to scale K_c to a measured effective (over-capillary) saturation $K_{eff,sat}$. Since $K_{c,cap}$ in the present work is predicted directly and not reliant on scaling by η_{cap} the model of Scheffler and Plagge is rewritten to Eq. (23).

$$K_c = \frac{f_l}{f_l(w_{cap})} K_{c,cap} K_{rel} \tag{23}$$

f_l, Eq. (24), being the scaling function of the mechanistic serial-parallel pore model described by Scheffler and Plagge [7], following the principles of Grunewald et al. [10], and $f_l(w_{cap})$ being f_l evaluated at w_{cap} (moisture content at capillary saturation).

$$f_l = \frac{\left(\frac{w}{w_{sat}}\right)^{\eta_{sp}}}{\left(\frac{w}{w_{sat}}\right)^{\eta_{sp}} + \left(1 - \frac{w}{w_{sat}}\right)^2 \left(1 - \left(\frac{w}{w_{sat}}\right)^{\eta_{sp}}\right)} \tag{24}$$

where η_{sp} is a parameter to adjust the serial-parallel relation, by modifying the volumetric fraction that is parallel pore domain in the mechanistic model [7], and w_{sat} is moisture content at saturation. K_{rel} being the relative capillary conductivity [7, 10] given as:

$$K_{rel} = \frac{\int_0^{\theta_c} p_c^{-2} d\theta_c}{\int_0^{\theta_{c,cap}} p_c^{-2} d\theta_c} \quad for\ \theta_c \le \theta_{c,cap} \tag{25}$$

In contrast to [7, 10] the upper integral limit below the fraction line is $\theta_{c,cap}$, instead of $\theta_{eff,sat}$. The η_{sp} parameter is material dependent [19]; however, we will argue it is also dependent on boundary conditions, i.e. dependent on whether it is absorption, redistribution or drying of moisture, or a combined representation of these, which is in focus when determining capillary conductivity (see Section 4.3). For a hypothetical pure parallel flow behavior $\eta_{sp} = 0$; however, usually it resides in the interval up in lower single digits.

2.6. Thin film model

Surface diffusion is a liquid transport mechanism which is important in pores not available for capillary transport, due to too low moisture filling for capillary menisci to form. Thin film flow is an approach to account for surface diffusion. We apply parts of the model approach described by Lebeau and Konrad [11]. Integration of a velocity distribution, arrived from Navier-Stokes equations, over a film thickness yields the volumetric flow rate per unit length of film cross section [11]. Adopted from [11], the thin film equation assuming no-slip at pore wall and negligible shear between liquid and air becomes:

$$\dot{V}' = \frac{\delta^3}{3\mu_w} \frac{dp_c}{dx} \tag{26}$$

where δ is the film thickness, which can be expressed as function of capillary pressure. Positive value for p_c gives Eq. (26) without minus sign in contrast to [11].

Multiplying Eq. (26) with the water density and the pore system void circumference over a cross section of the control volume gives the moisture flux:

$$j_{film} = \frac{\rho_w \delta^3}{3\mu_w} C_{\mathrm{int},v} \frac{dp_c}{dx} \tag{27}$$

where $C_{\mathrm{int,v}}$ is the circumference of internal voids not capillary filled as function of p_c, with $C_{int,v} = C_{int,v,tot} - C_{int,v,c}$, where $C_{int,v,tot}$ is the total circumference of internal voids and $C_{int,v,c}$ is the circumference of filled capillary pores. Ideally $C_{int,v,c}(p_c)$ should be found from a pore size distribution; however, if relying on the retention curve, as is done in the current paper, it can be calculated as:

$$C_{\mathrm{int},v,c} = \int_R 2\pi r \frac{dL}{dx} \frac{dn(r)}{dr \cdot dA} dr \overset{eq.(5)}{=} \frac{2}{B_A} \int_0^{\theta_c} \frac{1}{r} d\theta_c \tag{28}$$

$$C_{\mathrm{int},v,tot} = \frac{2}{B_A} \int_0^{\theta_{c,cap}} \frac{1}{r} d\theta_c \tag{29}$$

Note that Eqs. (28) and (29) provide the inscribed circle circumference of the capillaries, thereby constituting a simplification to film flow. The radius in Eqs. (28) and (29) is solved from Eq. (7), where B_c needs to be approximated by comparing measured A_w to Eq. (21). In lack of detailed information about the pore shapes, B_f, B_c and B_A are unknown. If values for B_f and B_A are chosen, based on simple assumptions, a value for B_c can be identified and Eqs. (28) and (29) can be calculated. We here assume film in over-capillary pores (not filled at capillary saturation) has negligible contribution to hydraulic conductivity, due to a relative low total circumference of such pores. These are therefore not included in the calculation. Furthermore, for the integration in Eqs. (28) and (29) we do not allow accumulated circumference for pores with radius below twice the diameter of a water molecule (diameter of a water molecule ≈ 3E-10 m) as no efficient film flow will allow to form for smaller pore sizes.

From Eq. (27) the film contribution to the hydraulic conductivity can be identified as:

$$K_{film} = \frac{\rho_w \delta^3}{3\mu_w} C_{\mathrm{int},v} \tag{30}$$

According to [11] the film thickness is involved in two relations of disjoining pressure components. The overall disjoining pressure is given as [11]:

$$\Pi(\delta) = \Pi_e(\delta) + \Pi_m(\delta) \tag{31}$$

where Π_e is the ionic-electrostatic component and Π_m the molecular component.

$$\Pi_e(\delta) = \frac{\varepsilon_r \varepsilon_0}{2} \left(\frac{\pi k_B T}{eZ} \right)^2 \frac{1}{\delta^2} \tag{32}$$

Table 1
Parameters for Eq. (32) and (33) adopted from [11].

Parameter	Description	Value
A_{svl} (J)	Hamaker constant	-6.0×10^{-20}
e (C)	Electron charge	1.60218×10^{-12}
k_B (J/K)	Boltzmann constant	1.38065×10^{-23}
T (K)	Temperature	293.15
Z (-)	Valence charge	1
ε_0 (C^2/(J m))	Permittivity of free space	8.85419×10^{-12}
ε_r (-)	Relative permittivity of water	80.23

$$\Pi_m(\delta) = -\frac{A_{svl}}{6\pi\delta^3} \tag{33}$$

with parameters summarized in Table 1, assessed at 293.15 K.

The disjoining pressure Eq. (31) is related to liquid pressure [11]:

$$\Pi(\delta) = p_g - p_l \tag{34}$$

Relating Eq. (34) to the capillary pressure which is also defined $p_c = p_g$ - p_l one have that the disjoining pressure is analog to capillary pressure.

Since Eqs. (32) and (33) are functions of δ^{-2} and δ^{-3} respectively, it is inconvenient to analytically solve for δ. Instead, for simplicity we propose calculating $\Pi(\delta)$ for a range of δ and then plot $\log(\delta)$ as function of $\log(\Pi(\delta))$. From such a plot a simple 2nd degree polynomial function can be fitted. Following this approach δ can be approximated with:

$$\delta_{film} = 10^{0.0116\cdot(\log|p_c|)^2 - 0.5535\cdot\log|p_c| - 5.7810} \tag{35}$$

Eq. (35) has up to ± 5% deviation to the actual film thickness over the range $10^0 < |p_c| < 10^9$ Pa. The film model, Eq. (30), could seemingly model hydraulic conductivity in the hygroscopic region for non-filled pores. However, with its background stemming from the rather macroscopic perspective of solving Navier-Stokes, it lacks in handling complexity associated with very thin films at nanoscale. For very thin films, measuring in a low number of water molecule layers, limiting aspects, physical conditions, material properties and pore wall characteristics will impact film existence and behavior. For instance, 1) water molecule diameter limits lowest film thickness and smallest pores that are effectively accessible to water, 2) material hydrophilicity or hydrophobicity, temperature, film confinement, and pore wall roughness affect water molecule orientation, structuring of the fluid, adhesion forces, no-slip tendency at pore wall and fluid properties such as density and viscosity, e.g. [23, 27].

Therefore, there is need for corrections to the film model, or a more advanced film model altogether, to address nanoscale properly. However, instead of adding complexity to the film model, such as to some extent is done in [11], we circumvent the issue with two simple/practical correctional steps; 1) the film thickness cannot be thicker than what the adsorbed water content in the material allows for. Hence, the overall film moisture content (adsorbed part of retention curve) divided by the product of water density and the pore system surface area of non-filled capillaries gives an upper bound. 2) in the lower to middle hygroscopic region we keep the hygroscopic model from Scheffler and Plagge, described in next subchapter, with a smooth transition from the hygroscopic model to the film model as function of relative humidity (RH). By taking these two steps the modeling is kept simpler, but at a cost of realism and accuracy.

With step 1), resulting film thickness to be applied in Eq. (30) becomes:

$$\delta = \min\left(\delta_{film}(p_c), \frac{w(p_c) - w_c(p_c)}{\rho_w C_{\text{int},v}(p_c)}\right) \tag{36}$$

Or

$$\delta = \min\left(\delta_{film}(p_c), \frac{w(p_c) - \rho_w B_A A_{\text{int},v,c}}{\rho_w C_{\text{int},v}(p_c)}\right)$$

where w_c is the capillary retained moisture content occupying filled capillaries, and $A_{int,v,c}$ the cumulative inscribed circle cross sectional area of filled capillaries given by Eq. (37), derived in same way as Eq. (28).

$$A_{\text{int},v,c} = \frac{1}{B_A}\int_0^{\theta_c} d\theta_c \tag{37}$$

2.7. Hygroscopic correction model

Scheffler and Plagge [7] propose accounting for liquid conductivity in the hygroscopic region by assessing the difference in vapor diffusion between dry cup and wet cup measurements. Herein they assume a negligible liquid transport contribution included in the vapor conductivity K_v (Eq. (38) [1]) for the dry cup measurement. The difference; wet cup – dry cup, Eq. (39), approximates the liquid transport fraction K_{hyg} acting during the wet cup measurement. They propose three vapor diffusion measurements are needed to enable logarithmic interpolation and extrapolation: one dry cup and two different wet cup measurements. Eq. (38) arise from relating vapor diffusion to a driving potential on the form of capillary pressure.

$$K_v = \frac{\delta_{v,a}}{\mu}\cdot\frac{\phi p_{v,sat}}{\rho_w R_w T} \tag{38}$$

where $\delta_{v,a}$ is the vapor diffusion coefficient of air, μ the vapor diffusion resistance factor, $p_{v,sat}$ the saturated vapor pressure.

$$K_{hyg}(\theta_{wet}) = \left(\frac{\phi(\theta_{wet})_{wet}}{\mu_{wet}} - \frac{\phi_{dry}}{\mu_{dry}}\right)\delta_{v,a}\frac{p_{v,sat}}{\rho_w R_w T} \tag{39}$$

where θ_{wet} is the associated volumetric moisture content at which K_{hyg} is determined, μ_{wet} and μ_{dry} are vapor diffusion resistance coefficients from wet and dry cup measurements, and ϕ_{wet} and ϕ_{dry} effective RH associated with respective resistance coefficient. Commonly ϕ_{wet} = 0.715 and ϕ_{dry} = 0.25 since μ_{wet} and μ_{dry} are respectively found at standardized conditions 50/93% and 0/50% RH [28].

Unfortunately, usually only a single wet or dry vapor diffusion resistance (in Europe commonly defined by [28]) is sought. Rarely more than one of these is reported in a study. Carmeliet and Roels [1] is one of few exceptions explicitly having reported three measurements (one dry cup and two wet cup). Therefore, three measurements need to be preplanned with determining K_{hyg} in mind. If only one of the resistance coefficients is available, for instance the dry cup, then the other one associated with ϕ_{wet} = 0.715 could be subjected to a guesstimate. For materials having very low hygroscopicity, i.e., relatively small difference in sorption between 25% and 71.5% RH, one can assume μ_{wet} and μ_{dry} to be rather similar. If only one or two values are available one can adopt K-values from the thin film model at relatively high RH values, as long as these are larger values than the one or two values of the liquid part of vapor conductivity which are available. If the thin film model gives larger μ-equivalent values (Eq. (38) solved for μ from K_{film}) than μ_{dry} we recommend setting successively slightly lower vapor diffusion resistance factors for the two wet cup calculations of Eq. (39), (e.g. $\mu_{wet} = \mu_{dry}$ - *0.1*). Then, logarithmic interpolation still can be achieved.

A 2nd degree Lagrange logarithmic interpolation, incorporating an arbitrary third liquid conductivity point; $K_{hyg}(\phi_{dry}) = 10^{-2}K_{v,dry}$, could be a practical and reasonable approach for interpolation.

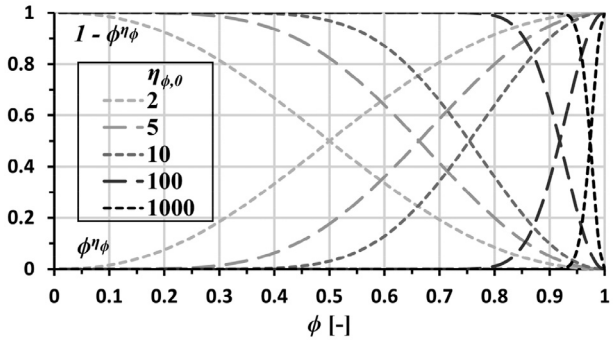

Fig. 1. Influence of $\eta_{\phi,0}$ on the transition between hygroscopic correction model and film/capillary models.

2.8. Proposed hydraulic conductivity model

The resulting model is in general a combination of the liquid conductivity model from Scheffler and Plagge [7] and the thin film model of Lebeau and Konrad [11]. However, it includes a significant key alteration by having replaced $K_{eff,sat}$, i.e. measured effective saturated conductivity, with the prediction expression for $K_{c,cap}$, which instead requires measurement of A_w. Saturated capillary conductivity measurements are relatively more complicated than measurements of the capillary absorption coefficient. Furthermore, the scaling parameter η_{cap} of the Scheffler and Plagge model is avoided, which significantly simplifies the calculation procedure, since this parameter is determined iteratively by simulation of water absorption experiments [7]. The new overall model is given as:

$$K = (1-\phi^{\eta_\phi})K_{hyg} + \phi^{\eta_\phi}\left(K_{film} + K_c\right) \tag{40}$$

where η_ϕ is a fitting exponent function, which we have arbitrarily given the form $\eta_\phi = \eta_{\phi,0}(1-\phi)$, where $\eta_{\phi,0} \geq 0$. Setting $\eta_{\phi,0} = 0$ would remove impact of the hygroscopic correction model and would require a more sophisticated thin film model as discussed in Section 2.6. Fig. 1 illustrates the impact of the function depending on $\eta_{\phi,0}$. With $\eta_{\phi,0} = 5$ a rather balanced transition within the upper hygroscopic region is achieved between the hygroscopic correction model and the film/capillary models, whereas higher values will ensure the hygroscopic correction model overrides more of the hygroscopic region. Note that Eq. (40) needs to be supplemented with a criterion which ensures K increases or remains constant as the capillary pressure decrease in order to avoid potential cases where the transition from the hygroscopic correction model to the film and capillary models results in a fall in hydraulic conductivity. Relevant for some materials where the film model provides lower predictions than the hygroscopic correction model.

Eq. (40) ensures that K_{hyg} is phased-out while K_{film} is phased-in as ϕ increase. Furthermore, since K_{film} is dependent on $C_{int,v}$, which subsides as capillary pores are filled, the capillary model takes over for K_{film} as this happens. Since both ϕ and θ can be expressed as functions of p_c Eq. (40) can readily be applied to generate a $\log(p_c)$ – $\log(K)$ table for implementation by logarithmic interpolation in hygrothermal simulation models (equal to the setup of the Hamstad 4 benchmark [29]).

2.9. Retention curve

The retention curve consists of an adsorptive and a capillary contribution, w_{ad} and w_c respectively:

$$w = w_{ad} + w_c \tag{41}$$

It is of interest to separate the two contributions to separately control the adsorbed and capillary related moisture contents for implementation in hydraulic conductivity sub-models. Different models have been proposed for the retention curve contributions of Eq. (41) in the literature, e.g. [11, 12, 30]; however, these become difficult to apply in the present work. In [11] one rely on an unknown adsorbed moisture content (hypothetical bound film in both capillary filled and non-filled pores) θ_0 at a matric head of −1 m. From our experience it is difficult to determine θ_0 from retention curve data and to get the function it resides to fit the retention curve of certain materials, even though the overall procedure in [11] for determining w_{ad} and w_c is elegant. In [12] and [30] the adsorbed moisture content is not replaced by capillary filling, which would cause underestimation of w_c at higher moisture contents. Since we base the capillary conductivity on Hagen-Poiseuille equation, we require the initially adsorbed moisture content on pore walls to be transformed into capillary moisture content as capillary menisci are formed, filling the entire cross section with moisture as capillaries become saturated. Consequently, we have had to choose a different approach.

The approach for handling the retention contributions depend on whether the pore size distribution or only the retention curve is available. With the pore size distribution available, one can estimate the adsorbed moisture content as the product of the film thickness, the non-capillary-filled pore surface area and the water density, accounting for moisture reduction due to film curvature. If only relying on the overall retention curve, which is the case in the current work, we propose the following approximation approach.

For implementation of the current model a retention expression proposed by Carmeliet and Roels [31] was made multimodal; resulting in Eq. (42). The expression is based on the Van Genuchten expression [5] proposed to be used multimodal by Durner [9], and extended with a Freundlich type expression [32].

$$w = w_{\lim}\left[\exp\left(-\frac{p_c}{\rho_w R_w T}\right)\right]^{n_{w,0}} + (w_{cap} - w_{\lim}) \cdot \sum_{i=1}^{N=4}\left(l_{w,i}\left[1+(c_{w,i}\cdot p_c)^{n_{w,i}}\right]^{\left(\frac{1-n_{w,i}}{n_{w,i}}\right)}\right) \tag{42}$$

where w_{lim} would be the limiting, critical water content between the hygroscopic and over-hygroscopic region (however, the actual w_{lim} value could be expected to deviate from the critical moisture content, being a more arbitrary fitting parameter [31]), $n_{w,0}$ fitting exponent, $l_{w,i}$ weighing coefficient equal to share of pore volume associated with corresponding inflection point in a cumulative pore size distribution, i.e. $\Sigma\ l_{w,i} = 1$, $c_{w,i}$ inverse of p_c at inflection point, $n_{w,i}$ fitting exponent.

In Eq. (42), the Freundlich term associated with w_{lim} is intended to provide the adsorptive contribution at low to intermediate RH-values, before capillary filling becomes significant, while the Van Genuchten term associated with w_{cap} - w_{lim} being the multimodal expression for capillary retained moisture. Of course, this is an over-simplification where in reality adsorbed moisture would be present at higher moisture contents in pores not yet capillary filled, whereas part of the initial adsorbed moisture content would become part of capillary filled pores. Furthermore, some materials, for instance concrete, have such a small pore structure that both film adsorption and capillary filling are significant at intermediate RH-values. Hence, respectively associating the Freundlich term and Van Genuchten terms to adsorptive and capillary moisture is not feasible in a general approach for all materials.

We therefore apply an iterative procedure:

1. Integrate all sub model integrals over θ instead of θ_c, with θ derived from Eq. (42) as $\theta = w/\rho_w$.
2. Calculate $\delta_{film}(p_c)$ Eq. (35) and $C_{int,v} = C_{int,v,tot} - C_{int,v,c}$ with Eqs. (43) and (44), which now include a curvature correction factor $f_{curvature} = (\pi r^2 - \pi(r-\delta)^2)/(2\pi r\delta)$ for $\delta < r$ and $f_{curvature} = \pi r^2/(2\pi r\delta)$ for $\delta \geq r$.

Table 2
Description details on model datasets.

	Input data availability			Hydraulic model dataset derived from a combination of			
Material [source]	Sorption curve	Retention curve	Vapor resistance measurements	Direct measurements	Modeled	Adjusted from indirect measurements	Post-processed from simulation
Brick [19]	yes	yes[a]	1 reported	K_{sat} only	yes	yes	yes
Sand-lime brick [19]	yes	yes[a]	1 reported	K_{sat} only	yes	yes	yes
Aerated concrete [19]	yes	yes[a]	1 reported	K_{sat} only	yes	yes	yes
Calcium silicate insulation [19]	yes	yes[a]	1 reported	K_{sat} only	yes	yes	yes
Brick [1]	yes	yes	3 reported	K_{sat} only	yes	yes[c]	no
Sand-lime brick [1]	yes	yes	3 reported	K_{sat} only	yes	yes[c]	no
Brick [33]	no	yes	1 reported, 3 K_v plotted	yes[b]	no	yes[c]	no
Cement mortar (wet cured) [33]	no	yes	1 reported, 3 K_v plotted	yes[b]	no	yes[c]	no
Calcium silicate insulation [34]	yes	yes	1 reported	K_{sat} only	yes	no	no
Limestone [35]	no	function	1 reported	no	yes	yes	no
Concrete [36, 37]	yes	yes	none	K_{sat} only	yes	no	no

[a] retention curve for adsorption is in the source presumed from measured retention curve for desorption.
[b] x-ray measurement data.
[c] only hygroscopic region.

3. Calculate $w_{ad}(p_c) = \rho_w C_{int,v} \delta_{film}$ as an approximation of film bound moisture.
4. Calculate $w_c(p_c) = \max(0, w - w_{ad})$ with w from Eq. (42).
5. Recalculate all integrals with $\theta_c = w_c/\rho_w$

$$C_{\text{int},v,c} = \frac{2}{B_A}\int_0^{\theta_c} f_{curvature}\frac{1}{r}d\theta_c \tag{43}$$

$$C_{\text{int},v,tot} = \frac{2}{B_A}\int_0^{\theta_{c,cap}} f_{curvature}\frac{1}{r}d\theta_c \tag{44}$$

3. Application and evaluation procedure

3.1. Datasets

Datasets are chosen from the literature to assess the model and alternative approaches for comparison. The datasets include: brick, sand-lime brick, aerated concrete and calcium silicate insulation from Scheffler [19], ceramic brick and calcium silicate brick (sand-lime brick) from Carmeliet and Roels [1], brick and wet cured cement mortar from Derluyn et al. [33], calcium silicate insulation from Häupl et al. [34], limestone from Cabrera et al. [35], and concrete (labeled 65DI) from Leech [36, 37]. It is important to point out that these datasets are not purely experimental datasets, rather they provide hydraulic conductivity curves derived from varying degree of being modeled and fitted to direct or indirect experimental data of a material's hydraulic conductivity. Therefore, they will henceforward be referred to as model datasets. In their respective sources, the model datasets have gone through some experimental validation on absorption [1, 33-35, 37] and drying [1]. Generally, only model datasets which include necessary input data; retention curve (adsorption), capillary absorption coefficient (or sorptivity), vapor resistance coefficient (or vapor diffusion coefficient), and a proposed model/dataset for the hydraulic conductivity have been chosen. However, concrete is also included even though the source does not include vapor resistance data. Hence, for concrete, only the capillary conductivity will be assessed. Table 2 includes additional details on the model datasets. Of the models datasets, those of Scheffler [19] give hydraulic conductivity which is intended to be valid both for absorption and drying, whereas the rest address absorption only. It should also be noted that the retention curves from Scheffler do not stem from direct measurements for the most part, rather Scheffler estimated them from experimentally determined desorption retention curves and assessment of material pore structure [19].

Table 3
Tortuosity values.

Material	N	τ [-]	ε [%]	Ref.
Brick	15	1.6–5.4	18.8–39.0	[39]
	1	2.654	26	[40]
Aerated concrete	8	1.4965–1.7818	72.4–83.8	[41]
Calcium silicate insulation	–	1.092[a]	90	–
Sand-lime brick	1	2.085	33	[40]
Limestone	2	1.27,1.47	24.3,32.1	[42]
Cement mortar	1	2.875	15.6	[40]
Concrete	1	3.536	13.4	[40]

[a] calculated from tortuosity expression derived by Yu and Li [38], based on 90% porosity.

3.2. Practical implementation of the hydraulic model

The relation between p_c and θ for each material is given by the retention curve accompanying each dataset. Since it is rather inconvenient to solve p_c from Eq. (42), integration of integrals containing p_c is done numerically after ensuring sufficiently high resolution in values of w being evaluated. For instance, in a spread sheet, enough values of w need to be calculated to accurately capture the shape of p_c as function of θ. The retention curves have been generated from Eq. (42) with input parameters which can be found in Appendix A, and give approximately identical retention curves to what accompanying the datasets.

In addition to input obtained from dataset sources, material tortuosity is needed to solve Eq. (21) (without the correction factors, see Section 2.6). Approximations to tortuosity can be found from values reported in the literature. Some values are summarized in Table 3, with the average (Table 4) applied in present work (except with exclusion of the highest outlier of brick). Although there is a distinction between geometric, electrical, diffusive and hydraulic tortuosity [14], such a distinction has not be addressed in the present work. The uncertainty and inaccuracy of applying literature values for tortuosity to specific materials is assumed to be greater than the distinction between the different definitions of tortuosity. The distinction becomes more important if the tortuosity is measured specifically for respective materials. A correlation to porosity is often attributed the tortuosity [14], however we have not differentiated the tortuosity by porosity for the materials of the same type, e.g. brick. In absence of tortuosity values a geometrical tortuosity model derived by Yu and Li [38] can be used as an approximation. It has the benefit of not requiring any empirical parameters or physical characteristics, except the porosity. However, it does not represent any natural porous material [14].

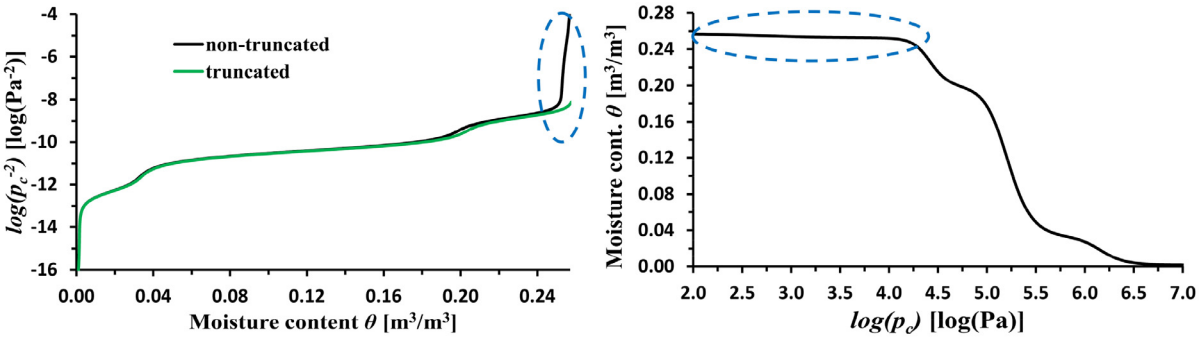

Fig. 2. Left: principle of truncated area under the curve for brick (Scheffler). Encircled region highlights the area under the curve in which p_c rapidly decrease over the last few % of retained moisture content. Right: corresponding retention curve, with the challenging region encircled.

Table 4
Chosen values for parameters not available from dataset sources.

Material	τ	B_f	B_A	η_{sp}[a]	$\eta_{\phi,0}$
Brick Derluyn	2.7	1.43	1.27	1	5
Brick Carmeliet	2.7	1.43	1.27	1	5
Brick Scheffler	2.7	1.43	1.27	2[b]	5
Sand-lime brick Carmeliet	2.1	1.43	1.27	1	5
Sand-lime brick Scheffler	2.1	1.43	1.27	2	5
Calcium silicate Scheffler	1.1	1.43	1.27	1	5
Calcium silicate Häupl	1.1	1.43	1.27	1	5
Limestone	1.4	1.43	1.27	1	5
Aerated concrete	1.7	1.43	1.27	2	5
Cement mortar	2.9	1.43	1.27	1	5
Concrete	3.5	1.43	1.27	1	5

[a] The choice of η_{sp} is discussed in subchapter 4.3.
[b] a value of 2.8 is specified in [7]; however, this value seemingly becomes too high, see Section 4.1 and 4.3.

For simplicity we have chosen a square pore shape for the correction factors B_f and B_A. A square pore shape provides a perceived middle ground between an unrealistic ideal of cylindrical pore shape and more irregular pore shapes. Ideally the representative pore shape of each material should be assessed individually; however, this is left outside the scope of the current study.

The serial-parallel exponent η_{sp} of the mechanistic scaling function, Eq. (24), has been simply chosen as follows: $\eta_{sp} = 2$ for comparison to the model datasets from Scheffler [19], since these incorporate drying data. Exception is calcium silicate for which the model dataset correlates very well with perceived absorption behavior. For the rest of the datasets $\eta_{sp} = 1$. The choice of η_{sp} is made after experience with the model and with an aim to demonstrate the model from simple generalized inputs and not involve material dependent adjustment. Further assessment of η_{sp}-optimalization is addressed in Section 4.3.

Finally, for practical reasons the integrals of $p_c^{-1/2}$ and p_c^{-2}, Eqs. (21) and (22), have been truncated at a slightly lower moisture content than $\theta_{c,cap}$. The reason for this can best be explained with Fig. 2, where p_c^{-2} is plotted against moisture content. For the last few % of moisture content the function increases dramatically. Since the scale is logarithmic, an integration of the area under the curve will easily be heavily influenced by this area. Comparing to the retention curve, this moisture content corresponds to the last filling of large-scale capillary pores as the retention curve slope flattens out towards w_{cap}. As this occurs p_c-values decrease dramatically with only little change in moisture content. We will argue that this span in p_c-values is a poor representation of acting p_c associated with capillary absorption because:

- The large pores (pore volume) this moisture content represents have a high probability of being insufficient to represent continuous capillaries through the material.
- Certain materials have larger isolated pores which may be detected in measurements of retention curve or pore size distribution due to small scale samples, while for larger material scales the pores are not continuous through the material.

A similar discussion is given by Durner [8, 9] for the asymptotic slope of the retention curve near saturation for models including over-capillary retention. Although Durner [9] relates part of the issue to difficulty and uncertainty in determining the retention curve in the over-capillary region close to saturation, the high sensitivity of bundle of tubes *K*-models to low capillary pressures associated with the retention curve at high saturations remains an issue also here. For these reasons the integrals are truncated at a $\theta_{c,cap}$ cut-off value. For most materials this cut-off is above 97% of $\theta_{c,cap}$, with the brick (Carmeliet) at 95.7% due to a presumed lower precision in its retention curve compared to the other materials. The procedure has been kept simple, cutting the curve off where it starts turning upwards for the almost vertical increase (Fig. 2). Each integral is then divided by the cut-off value (e.g., if 98% then divided by 0.98). The resulting area under the curve is given by the truncated curve in Fig. 2.

3.3. Alternative approaches for comparison

A common alternative approach is that of calculating the hydraulic conductivity from the moisture diffusivity (e.g. [43, 44])

$$K_{Dw} = D_w \frac{dw}{dp_c} \tag{45}$$

The notation $_{Dw}$ in K_{DW} is here just applied to distinguish the hydraulic conductivity in Eq. (45) from Eq. (40). A much used empirical model for D_w is that of Künzel [45]:

$$D_{w,abs} = 3.8\left(\frac{A_w}{w_{cap}}\right)^2 1000^{\frac{w}{w_{cap}}-1} \tag{46}$$

The first part of Eq. (46); $3.8(A_w/w_{cap})^2$, is with the value 3.8 presumably a generalization of an integral of the area under a moisture penetration profile, see [46]. Several non-generalized expressions also exists, e.g. [46, 47]; however, these require a material dependent parameter. Note that Künzel [45] and Kruβ [48] distinguish between absorption and redistribution/drying, with $D_{w,red}$, based on experimental support, often presumed equal to $10^{-1}{\cdot}D_{w,abs}$.

An unfortunate consequence of Eq. (45) is the decrease of *K* when the retention curve flattens out over an interval of p_c. Carmeliet et al. [43] noted there is need for a correction to the resulting curve of *K* at low p_c-values to avoid a decrease in *K* which would be unphysical. They state *K* should monotonically increase with decreasing p_c (increasing moisture content) and propose to keep *K* constant after its highest value for successive decrease in

p_c. However, it is not only at low p_c-values decrease in K can occur with Eq. (45). It can also occur at intermediate p_c-values with retention curves for materials with a pore size distribution including distinctly different scales. See resulting graphs in Section 4.1. We therefore propose an algorithm for a modified calculation of the K_{Dw} curve:

$$K_{Dw,\,\mathrm{mod},i+1} = \begin{cases} K_{Dw,i+1} & for\ K_{Dw,i+1} \geq K_{Dw,\,\mathrm{mod},i} \\ K_{Dw,\,\mathrm{mod},i} & for\ K_{Dw,i+1} < K_{Dw,\,\mathrm{mod},i} \end{cases} \quad (47)$$

with i being an increment number representing the position in the resolution N of increasing moisture content, from $w = 0$ with $i = 1$ to $w = w_{cap}$ with $i + 1 = N$. Both K_{Dw}, Eq. (45), and $K_{Dw,mod}$, Eq. (47), are included for comparison, respectively referred to as *K(D_w absorption) standard* and *K(D_w absorption) modified* in graph legends.

The empirical prediction expression $K_{c,cap} = 10^{-8}\eta_{Aw}A_w{}^2$ reported by Scheffler [19], coupled with the overall hydraulic model through Eqs. (23) and (40), is also included for comparison. Since the material-specific η_{Aw} is unknown, the reported lower and upper bound of 0.95 and 16 respectively are both applied. The resulting hydraulic conductivity models are denoted *K model, empirical low* and *K model, empirical high.*

4. Results and assessment

4.1. Comparisons to datasets

Fig. 3, a) to k), presents the approaches to predict the material model datasets. Material input properties to the hydraulic model are given to the left while the results are compared to the model dataset on the right. Results of the hydraulic model proposed in this paper is labeled *K model, prediction*. For view on a log*(K)* – log*(p_c)* relation refer to Appendix B. Note that model dataset graphs of Fig. 3b), d) and j) also contain contribution from K_v while the prediction approaches do not. For the materials addressed in Fig. 3d) and j) particularly, which retain significant moisture in the hygroscopic region, comparison assessments at lower moisture contents are thus not viable.

Note that the results demonstrate the proposed prediction model with relatively generalized choices for input parameters (Table 4). Optimal fitting of these parameters for each material has not been a priority in this study. Nevertheless, a simple assessment of η_{sp} and $\eta_{\phi,o}$ is given in Section 4.3 and 4.4.

The *K(Dw absorption) standard* approach will not be addressed, as it is only included to illustrate the issue described in Section 3.3, while *K(Dw absorption) modified* is its replacement. The *K model, empirical low and high* are seen to vary greatly in their ability to align with the model datasets. The *low* only relatively close for sand-lime brick and calcium silicate, in Fig. 3e) and g) respectively. Whereas the *high* reasonable for all the three bricks, calcium silicate, and limestone in Fig. 3a), b), c), f) and h) respectively. For sand-lime brick, cement mortar and concrete both are far off (Fig. 3d) j) and k) respectively). Overall, in the expression $K_{c,cap} = 10^{-8}\eta_{Aw}A_w{}^2$ the material dependence is clearly not fully taken care of by $A_w{}^2$ alone; however, also the interval of η_{Aw} is insufficient and even lower values are needed to make it encompass cement mortar and concrete. Due to the unknown material dependent η_{Aw} from an a-priori perspective the *K model, empirical* approaches are not addressed any further.

In the remainder only *K model, prediction* and *K(Dw absorption) modified* are assessed.

Interestingly for both brick and sand-lime brick of the Carmeliet model datasets both approaches overestimate $K_{c,cap}$. This could indicate that the respective retention curves at high moisture contents encompass filling of pores which are rather isolated and not suitable to be included in the bundle of tubes model integral. However, for brick (Carmeliet) the retention curve also converges with a gentle slope towards w_{cap} over a longer interval of p_c compared to the other two bricks, which makes it more difficult to determine the truncation of the integrals for this material. The same issue is seen for aerated concrete. If for sand-lime brick (Carmeliet) the largest pores had not been included in the integrals (truncated at lower moisture content or with an adjusted retention curve) a better prediction of $K_{c,cap}$ could have been achieved. For sand-lime brick (Scheffler) and calcium silicate (Scheffler) it might be that Scheffler's estimate of the retention curves at low p_c-values provides too gentle slopes, when comparing to the desorption retention curves in [19]; however, the $K_{c,cap}$ prediction deviation could also be that the largest pores are too spatially sparce to resemble continuous capillaries.

One clear observation is how the *K model, prediction* given $\eta_{sp} = 1.0$ has a tendency to follow *K(Dw absorption) modified* for all materials. Due to the relative simplicity of the film model and the hygroscopic correction model, including increased uncertainty regarding the dataset models in the corresponding moisture region, as some are post-modified in this region, while others are not or seemingly not properly modeled in this region, it is hard to provide a concise and meaningful visual assessment of the figures in the hygroscopic region. However, it is included in a quantified assessment in the next section.

4.2. Quantified assessment

An attempt is made to quantify the prediction accuracy of the proposed hydraulic conductivity model to that of the model datasets. We introduce a factor of deviation f_d which will describe the average deviation from the reference model dataset. By average deviation a graph y_i will on average follow the notional relation $y_i = f_d{}^{\pm 1} y_{ref}$, where y_i and y_{ref} are respectively the y-values of the graph that is compared and of the reference graph it is compared to (i.e., the model dataset). The ± 1 exponent indicates the function y_i can both overshoot and undershoot function y_{ref}. To what extent under- or overshooting occurs is not divulged by the factor itself. Since the curves have a strong exponential nature, spanning many orders of magnitude, it is necessary to evaluate them in form of logarithms. The factor of deviation is given as Eq. (48). Note that the ± 1 exponent mentioned above is linked to taking the absolute value of the logarithmic difference.

$$f_d = 10^{\int_{\theta_{rel}} |\log(y_i) - \log(y_{ref})| d\theta_{rel}} \quad (48)$$

where $\theta_{rel} = \theta/\theta_{cap}$ is relative moisture content, i.e., relative to capillary saturated moisture content. If $f_d = 1.0$ the curves would be a perfect match; however. such a case would be highly unlikely. Although dependent on accuracy preference, values of $f_d \leq 2$ and $f_d > 2$ might respectfully be regarded as reasonable and not so reasonable predictions, with in mind the exponential nature of the capillary conductivity curve. Values of f_d <1.5 might be regarded as reasonably good.

Only the *K model, prediction* and *K(D_w absorption) modified* are assessed, since the former being the proposed hydraulic model and the latter is the likely (or common) contender. Overall, after assessing Fig. 3, the other approaches show to be less sophisticated and have less reliable performance. Factors of deviation are summarized in Table 5

Table 5 reveals the following. Hydraulic conductivity at capillary saturation is predicted better by *K model, prediction* in 5 materials, while better by *K(Dw absorption) modified* in 6 materials. For aerated concrete the two are almost equal, for limestone and cement mortar the two have both good predictions with rather high precision. Also, calcium silicate is similar for the two with fair precision, while for brick Carmeliet the two are similarly poor predic-

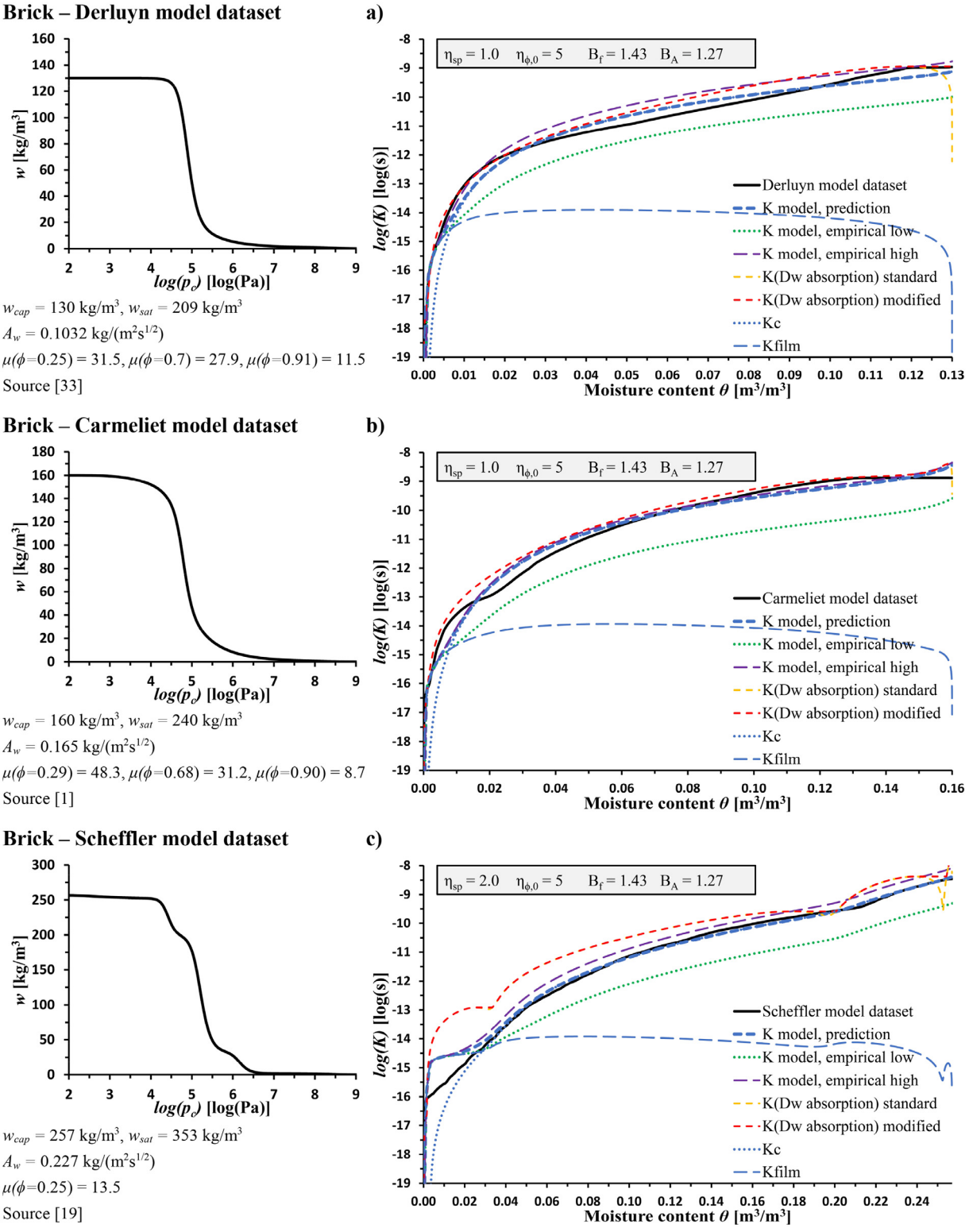

Fig. 3. Left: retention curves, reproduced with Eq. (42), and basic properties used as input in the hydraulic model. Right: hydraulic conductivity; different modeling approaches compared to datasets.

tions. Overall *K model, prediction* and *K(Dw absorption) modified* respectively have 8 and 7 reasonable predictions ($f_d \leq 2$), while both have 6 for reasonably good ($f_d \leq 1.5$).

Excluding the three materials at which *K(Dw absorption) modified* is at a disadvantage, each predict 4 materials better than the other over the whole moisture content interval. Furthermore, *K model, prediction* has 5 reasonably predictions while *K(Dw absorption) modified* has 6. For $\theta_{rel} \leq 0.5$, the numbers are 3 and 4 respectively while for $0.5 < \theta_{rel}$ 5 for both. Interestingly, there is only one reasonably good predictions for $\theta_{rel} \leq 0.5$, with *K model, prediction* only reaching the threshold value for Limestone, whereas for $0.5 < \theta_{rel}$ *K model, prediction* has 4 and *K(Dw absorption) modified* has 2. Summarized, *K(Dw absorption) modified* shows higher precision for a few more materials in $K_{c,cap}$ prediction, although the

Sand-lime brick – Carmeliet model dataset

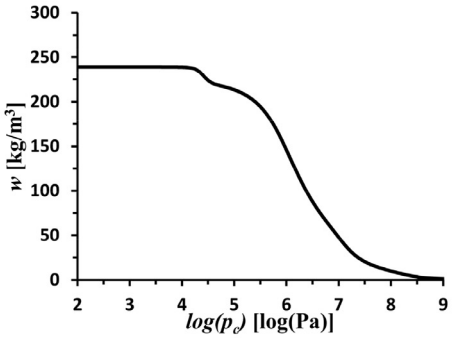

w_{cap} = 239 kg/m^3, w_{sat} = 319 kg/m^3

A_w = 0.043 kg/(m^{2}s$^{1/2}$)

$\mu(\phi$=0.3) = 23, $\mu(\phi$=0.7) = 12, $\mu(\phi$=0.92) = 3

Source [1]

d)

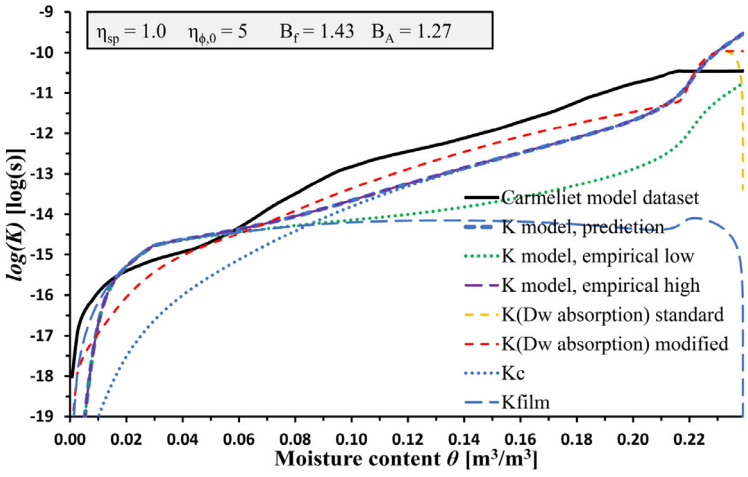

Sand-lime brick – Scheffler model dataset

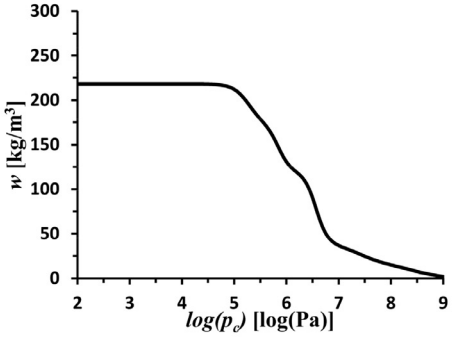

w_{cap} = 218 kg/m^3, w_{sat} = 345 kg/m^3

A_w = 0.052 kg/(m^{2}s$^{1/2}$)

$\mu(\phi$=0.25) = 40

Source [19]

e)

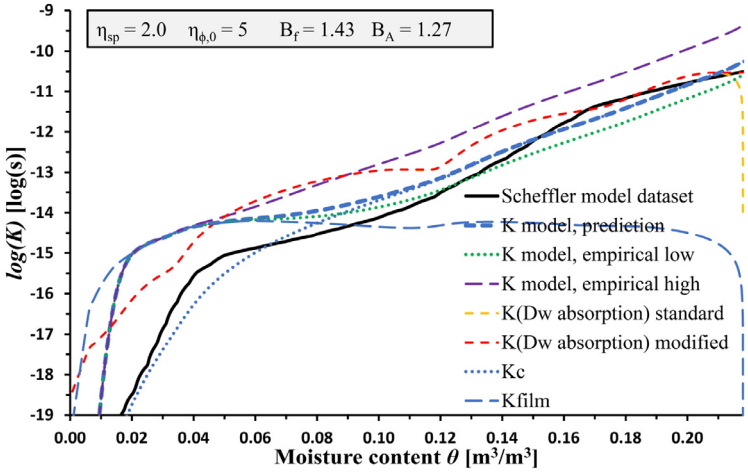

Calcium silicate – Scheffler model dataset

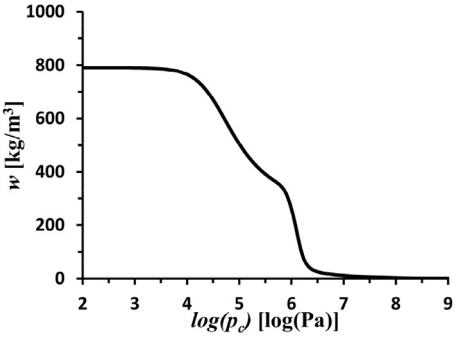

w_{cap} = 790 kg/m^3, w_{sat} = 900 kg/m^3

A_w = 1.11 kg/(m^{2}s$^{1/2}$)

$\mu(\phi$=0.25) = 4

Source [19]

f)

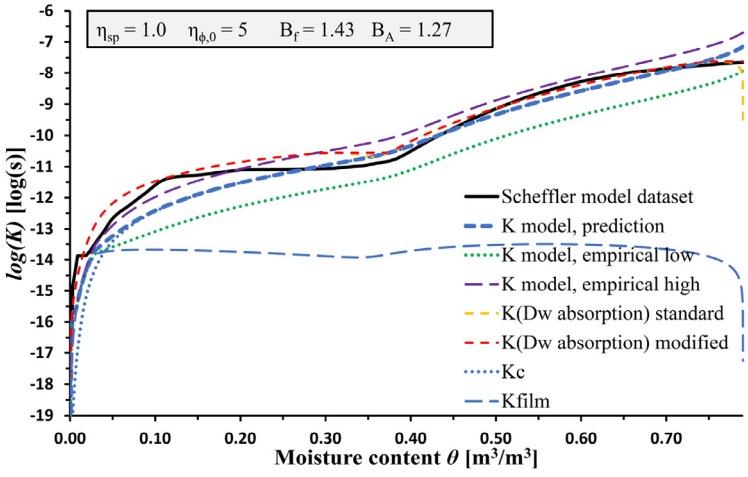

Fig. 3. Continued

Calcium Silicate – Häupl model dataset g)

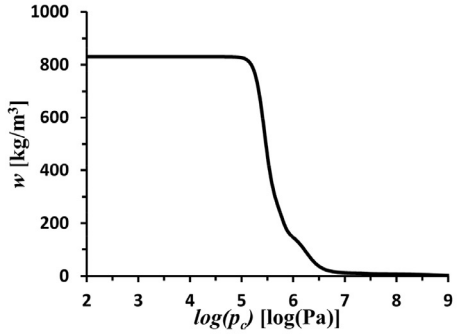

w_{cap} = 830 kg/m³, w_{sat} = 920 kg/m³
A_w = 1.19 kg/(m²s$^{1/2}$)
$\mu(\phi$=0.3) = 3.5
Source [34]

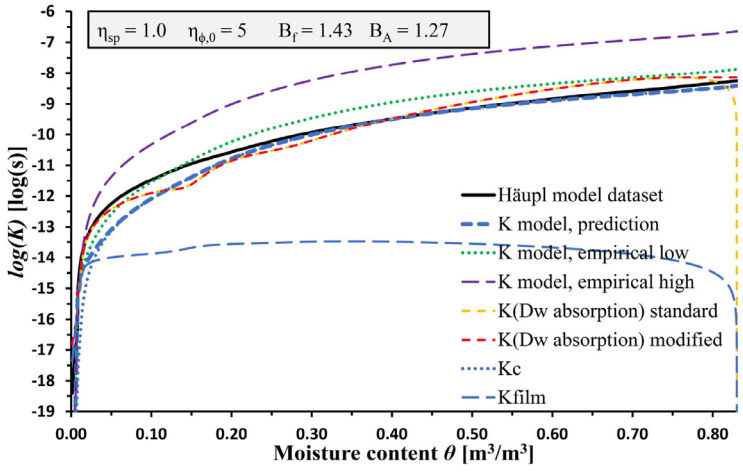

Limestone– Cabrera model dataset **h)**

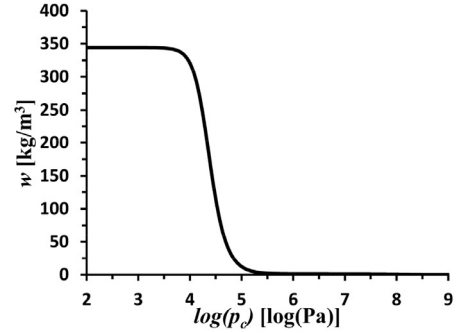

w_{cap} = 344 kg/m³, w_{sat} = 367 kg/m³
A_w = 1.009 kg/(m²s$^{1/2}$)
$\mu(\phi$=0.25) = 5
Source [35]

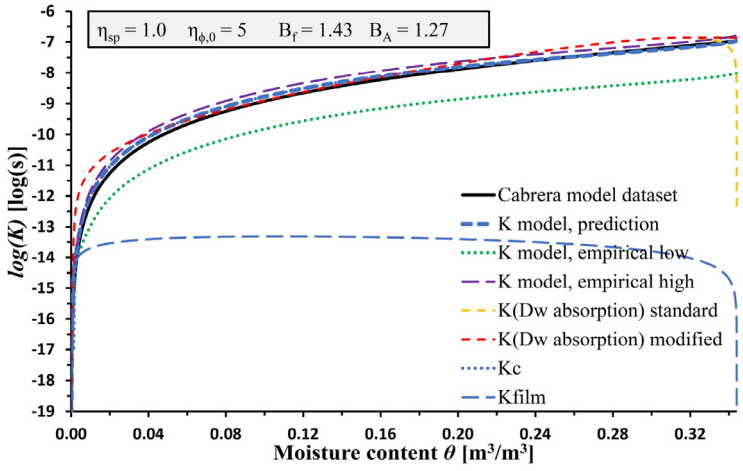

Aerated concrete – Scheffler model dataset **i)**

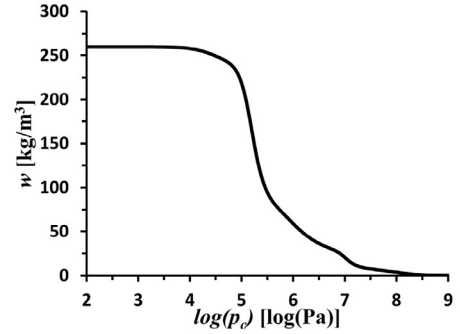

w_{cap} = 260 kg/m³, w_{sat} = 700 kg/m³
A_w = 0.043 kg/(m²s$^{1/2}$)
$\mu(\phi$=0.25) = 7.5
Source [19]

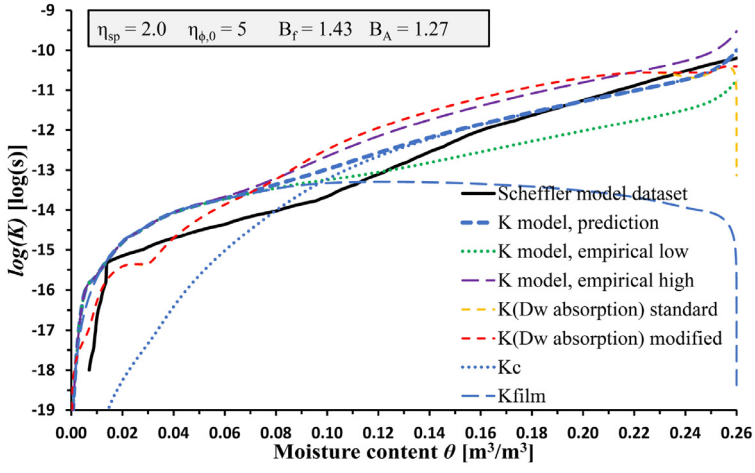

Fig. 3. Continued

difference is not great. On the other hand, *K model, prediction* provides higher precision for a few more materials in the upper moisture range. Even with these two distinctions in performance the two different approaches have similar overall performance, neither distinguish itself as especially better or worse compared to the other.

4.3. The η_{sp} parameter

The way the η_{sp} parameter influence the mechanistic serial-parallel pore model of [7] can be roughly be summarized as follows; With $\eta_{sp} \rightarrow 0$, hypothetically, the model becomes purely parallel, i.e. the capillaries involved in capillary transport are filled

Cement mortar – Derluyn model dataset

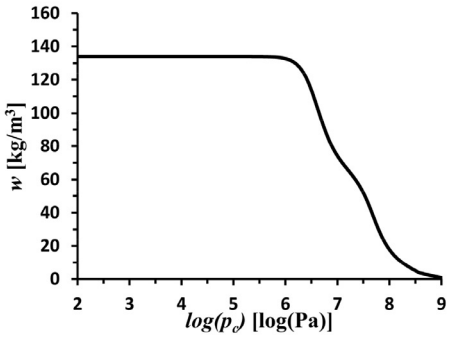

w_{cap} = 134 kg/m^3, w_{sat} = 158 kg/m^3

A_w = 0.0154 kg/(m^{2}s$^{1/2}$)

$\mu(\phi$=0.25) = 379, $\mu(\phi$=0.7) = 279, $\mu(\phi$=0.91) = 45.3

Source [33]

j)

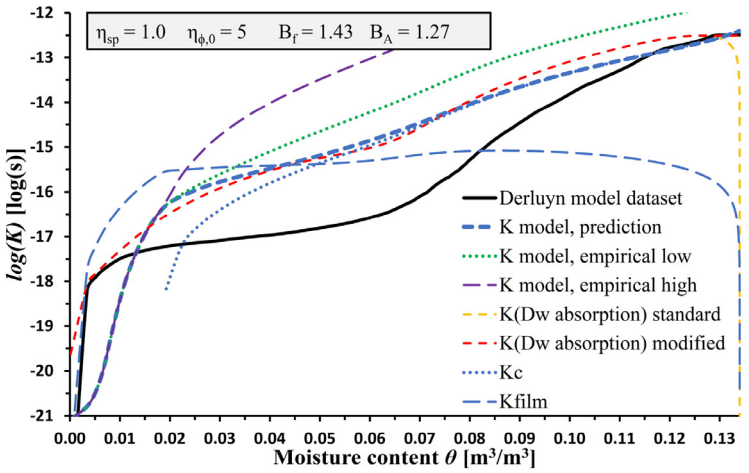

Concrete – Leech model dataset

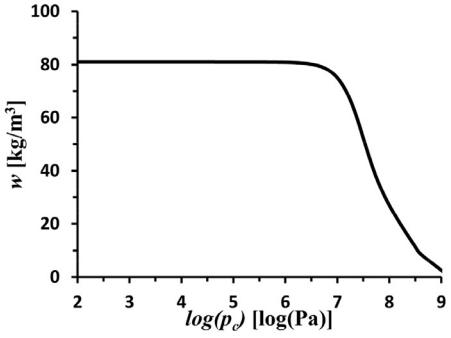

w_{cap} = 81 kg/m^3, w_{sat} = 127 kg/m^3

A_w = 0.00357 kg/(m^{2}s$^{1/2}$)

$\mu(\phi$=0.25) = ? (only capillary dataset)

Source [36, 37]

k)

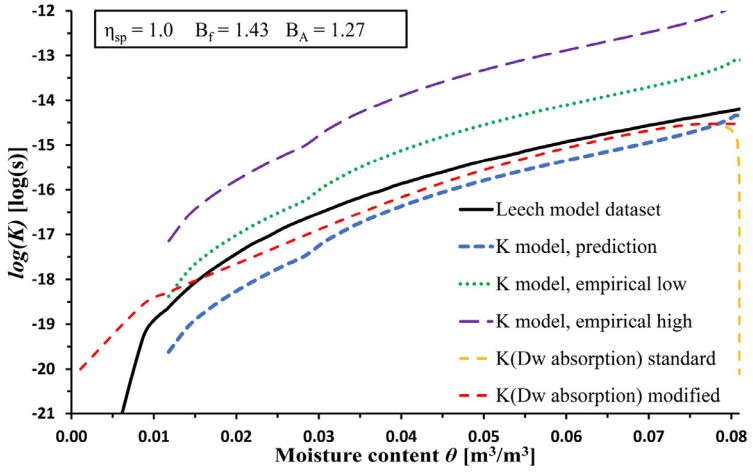

Fig. 3. Continued

Table 5
Quantified factors of deviation f_d, Eq. (48). Lowest deviation values in bold. Parentheses indicate where the *K(Dw absorption) modified* is at a disadvantage, i.e. model datasets adapted for drying.

	K model, prediction				K(D_w absorption) modified			
θ_{rel} integral interval	$0 < \theta_{rel} \leq 1$	$0 < \theta_{rel} \leq 0.5$	$0.5 < \theta_{rel} \leq 1$	$\theta_{rel} = 1$	$0 < \theta_{rel} \leq 1$	$0 < \theta_{rel} \leq 0.5$	$0.5 < \theta_{rel} \leq 1$	$\theta_{rel} = 1$
Brick Derluyn	**1.64**	1.75	**1.53**	1.44	1.93	**1.70**	2.18	**1.04**
Brick Carmeliet	**1.60**	**1.96**	**1.30**	**2.72**	1.77	2.32	1.35	3.03
Brick Scheffler	**(1.45)**	**(1.73)**	**(1.21)**	**1.18**	(5.20)	(12.63)	(2.14)	4.24
Sand-lime brick Carmeliet	4.51[a]	3.63[a]	5.60	8.17	**2.85**[a]	**2.71**[a]	**3.00**	**3.06**
Sand-lime brick Scheffler	**(5.34)**	**(17.60)**	**(1.62)**	1.81	(7.23)	(22.69)	(2.30)	**1.06**
Calcium silicate Scheffler	1.98	2.71	1.45	3.15	**1.62**	**2.12**	**1.23**	**1.08**
Calcium silicate Häupl	**1.57**	2.11	**1.17**	1.44	1.88	**1.96**	1.80	**1.29**
Limestone	**1.29**	**1.50**	**1.11**	**1.01**	1.76	1.75	1.77	1.28
Aerated concrete	**(2.60)**	**(4.68)**	**(1.45)**	**1.57**	(4.15)	(4.77)	(3.60)	1.60
Cement mortar	11.25[a]	27.99[a]	**4.52**	**1.19**	**8.69**[a]	**13.61**[a]	5.55	1.05
Concrete	3.11	4.80	2.40	**1.38**	**1.68**	**1.94**	**1.54**	2.11
# predictions $f_d \leq 2$	5 (6)	3 (4)	5 **(8)**	**8**	**6**	**4**	5	7
# predictions $f_d \leq 1.75$	**4 (5)**	2 **(3)**	**5 (8)**	7	2	2	3	7
# predictions $f_d \leq 1.5$	**1 (2)**	**1**	**4 (6)**	6	0	0	2	6
# predictions $f_d \leq 1.25$	0	0	**2 (3)**	3	0	0	1	**4**

[a] are significantly influenced by that the model dataset includes K_v contribution while prediction approach does not.

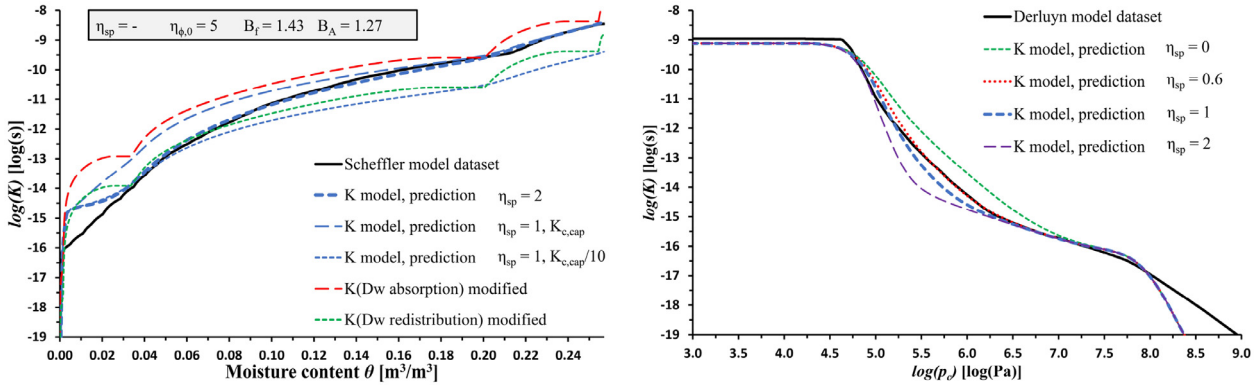

Fig. 4. η_{sp} parameter. Left: For brick (Scheffler), demonstration on how the η_{sp} parameter relates to absorption and redistribution. Right: For brick (Derluyn), demonstration of impact of variation in η_{sp}.

with continuous liquid towards some moisture front similar to an ideal imbibition model. With $\eta_{sp} = 1$ the model has a serial-parallel relation as function of *w/wsat*, Eq. (24), without diminishment or reinforcement though the exponent. Fig. 4 demonstrates the impact of the η_{sp} parameter. For datasets which unite absorption and drying data in one graph the result for brick (Scheffler) (Fig. 4 left) shows a value of $\eta_{sp} = 2$ is in good agreement; whereas, lime-sand brick (Scheffler) and aerated concrete are even better described by $\eta_{sp} = 3$ (not shown). Hence the results of Fig. 3 and Table 5 could be improved for these latter two materials updated with $\eta_{sp} = 3$. Consequently, based on the limited number of datasets which incorporate drying experiments we find $2 \leq \eta_{sp} \leq 3$ to best represent these. For the pure absorption datasets Fig. 3 has shown relatively good agreement with $\eta_{sp} = 1$. However, the choice of $\eta_{sp} = 1$ was a generalized one, and the best fit could deviate from this. Although the best fit on each dataset has not been investigated, Fig. 4 (right) demonstrates the impact of different η_{sp} on the brick (Derluyn), where a value of η_{sp} as low as 0.6 might give the better fit at lower moisture contents, although this cause poorer fit at intermediate moisture contents. Both the calcium silicate materials also indicate improvement with $\eta_{sp} = 0.6$ (not shown), or even perhaps slightly lower to $\eta_{sp} = 0.5$ for calcium silicate (Häupl). Except for concrete, which seems to best be modeled with $\eta_{sp} = 0$, no clear support is found for η_{sp}-values lower than 0.5 for the other datasets looked at. With only small improvement, limestone indicates values of η_{sp} up to 1.3 might be used (not shown). If excluding concrete, in lack of similar, confirming observations, then, based on the limited number of absorption datasets we find $0.5 \leq \eta_{sp} \leq 1.3$ to best represent these.

4.4. The $\eta_{\phi,0}$ parameter

As mentioned in Section 2.8 the $\eta_{\phi,0}$ parameter governs how much of the hygroscopic correction model overrides the film and capillary models in the hygroscopic region. Fig. 5 demonstrate how the $\eta_{\phi,0}$ parameter can be used to override the two other models for materials which has much of the retained moisture content within the hygroscopic region. For such materials there might be a conflict between the results of the film/capillary model and vapor resistance measurements which the hygroscopic correction model is built on. This conflicting behavior resembles the issue the η_{sp} parameter is designed to resolve. After all, the vapor resistance data is not related to absorption. Rather, it stems from steady state measurements. Still, η_{sp} and $\eta_{\phi,0}$ impact the overall model from different angles. For sand-lime brick (Carmeliet) changing $\eta_{\phi,0}$ to 200 would improve the fit to vapor resistance measurements (not shown). For the rest of the datasets too few vapor resistance measurements are known to give an assessment, or the materials retain too little moisture in the hygroscopic region for the issue to be relevant. We deem it outside the scope of this paper to investigate the correctness of combining data from "non-absorption" vapor resistance measurements with a capillary absorption prediction model.

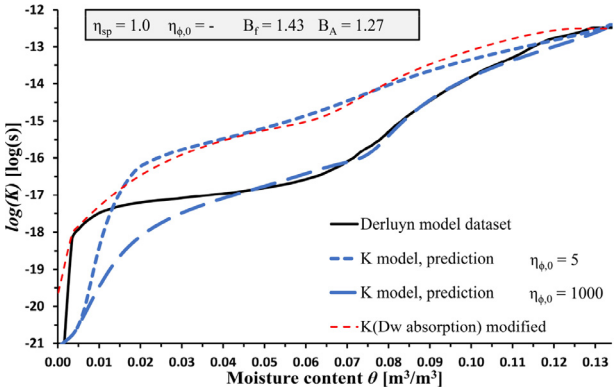

Fig. 5. Impact of the $\eta_{\phi,0}$ parameter on cement mortar. The deviation between the model dataset and the prediction with $\eta_{\phi,0} = 1000$ at low moisture contents stems from dataset including vapor conductivity (K_v).

5. Discussion

The proposed model has been demonstrated to be on par with the $K(D_w)$ approach. Nevertheless, since the model is sensitive to the capillary pressure of the largest pores it is important to combine the model with an assessment of whether the largest pore sizes can actually be believed to constitute continuous pores though the material. That is, whether the largest pores can be represented with the bundle of tubes model approach or whether they behave more isolated. The $K(D_w)$ approach is less sensitive on this aspect and therefore achieves better prediction of $K_{c,cap}$ for a few materials compared to the proposed model. However, at the same time the proposed model is seen to give better prediction in the higher moisture range as a whole. Consequently, there might be possible practical adjustments to the model application which can improve prediction performance, either 1) by a truncation at slightly lower moisture contents for materials with rather gentle retention curve slopes close to capillary saturation, or 2) by adjusting retention curves to become a bit more sharply rounded off at capillary saturation. Such adjustments have not been investigated in connection with the current study. It is also implicit that use of the model requires input of rather accurate retention curves. That is, retention curves for materials which do not have very uniform

pore size distribution should be described by multimodal curves which capture some resolution in the pore size distribution. Still, uncertainty persists regarding these issues since the current study has not investigated accuracy issues with retention curve representation and its effect on the model prediction performance.

Whereas traditional bundle of tubes models are criticized for having a non-physics based tortuosity correction [6, 49], the current model derivation has included the tortuosity leading up to Eq. (11). Nevertheless, for the current capillary model it turns out that the tortuosity is baked into the capillary absorption coefficient and is therefore not present in the final $K_{c,cap}$ prediction, Eq. (22). Another part of the criticism of bundle of tubes models is that they fail to increase the tortuosity of flow paths when the permeability decrease as water-filled pathways become sparse at low moisture contents [6]. The mechanistic model f_l (for its principle see [7]) does however address this issue even though it does not interfere with the tortuosity directly. If assessing Eq. (11) in connection with Eq. (23) one finds that K_c is proportional to f_l/τ^2 which could partly be interpreted in terms of providing an effective tortuosity which increase with lower moisture contents, since f_l decrease with lower moisture contents.

5.1. Other correction factors

With regard to calculating capillary absorption coefficients, Nikitsin and Backiel-Brzozowska [50] argues for a need to include additional correction factors. These include K_{NW} for taking into account *"narrowing and widening of capillaries along their length"*, K_T as a temperature correction to the ratio of σ_w/μ_w, based on a description of water vapor preceding the capillary moisture front where the vapor will adsorb on the pore walls, thereby releasing heat (this in capillary absorption experiments of initially dry materials), and K_μ for correcting the viscosity for its dependence on pore radius, mainly for $r < 1\ \mu$m [50].

Although K_{NW} has not explicitly been addressed in the present work we will argue both B_f and B_c implicitly could include such an effect. However, since the current model approach involves choosing a value for B_f, this effect is all placed in B_c when identified from comparing Eq. (21) to the experimentally determined A_w-value. Still, when estimating the pore radius with Eq. (7), the resulting r will be underestimated if B_c is significant influenced (diminished) from narrowing and widening of pores.

K_T can be calculated as $K_T = (\sigma_m \mu_0)/(\sigma_0 \mu_m)$, where subscripts *0* and *m* refer to ambient and microscale temperature respectively. This factor basically accounts for a reported microscale temperature increase which lowers the surface tension and viscosity. Although, Nikitsin and Backiel-Brzozowska [50] assume a 10 K increase for their case (with reported $K_T = 1.24$) they provide too little information to confidently generalize inclusion of such a factor. For instance, in order for a significant temperature increase to take place we would assume the following prerequisites are needed: 1) completely initially dry material, thereby creating high adhesion forces; hence, preconditioning to laboratory conditions of the material before A_w measurements cannot have taken place. 2) a large pore wall circumference to cross section area ratio is needed to give high heat release per water volume heated. 3) relatively fast capillary flow rate and low bulk material thermal inertia. We deem it outside the scope of the present work to address whether or to which degree such a phenomenon exists to give an impact, hence K_T is not included.

K_μ should ideally be included, since the factor is important for calculation of A_w, which when compared to measured A_w is used to approximate B_c and pore radius for the film model. In order to keep the model conveniently simple, and its description not too long, such a correction has not been included in the present work.

6. Summary and conclusions

Modeling capillary conductivity with a bundle of tubes model has been revisited. By incorporating the experimentally determined capillary absorption coefficient a novel prediction expression for the capillary conductivity at capillary saturation has been derived. By introducing a prediction of the conductivity at capillary saturation, bundle of tubes models become more directly implementable and avoid part of the criticism such models previously have received at over-capillary saturation. The feasibility of scaling bundle of tube models to conductivity at capillary saturation has been demonstrated.

A hydraulic conductivity model for the full moisture range has been established based on the Scheffler and Plagge model [7], supplied with a film model of Lebeau and Konrad [11]. With the new model no longer requiring iterative post-processing of a parameter for scaling to conductivity at over-capillary saturation, a simplification is achieved, easing applicability of the model. The impact of an adjustment parameter in the mechanistic scaling function, as part of the Scheffler and Plagge model, has also been demonstrated more in detail, which casts light on the flexibility of the model. Value interval recommendations for this adjustment parameter are provided. An additional adjustment parameter to adjust between the film/capillary models and a hygroscopic correction model (latter also being part of the Sceffler and Plagge model) has also been introduced and demonstrated to give some additional flexibility, although no conclusion has been made regarding its determination. As a necessary step towards the prediction expression for conductivity at capillary saturation a new analytical expression for the capillary absorption coefficient has also been derived. This derivation may provide contrasting nuances to previously reported derivations of this coefficient.

The new hydraulic conductivity model, including the new prediction expression for the conductivity at capillary saturation, has been demonstrated on 11 porous material datasets with reasonable success.

The resulting model should be easier to implement than most comparable, alternative bundle of tubes models by not requiring testing of capillary conductivity, since it utilize the easier determinable capillary absorption coefficient. The new prediction is however sensitive to the retention curve close to capillary saturation which for some cases could result in inaccurate prediction.

Also, although not new information, the article reaffirms that hydraulic conductivity is dependent on the situational boundary conditions, i.e., whether the material is subjected to absorption, redistribution or drying of moisture.

There is still much unanswered regarding how to more accurately and practically incorporate models for the hygroscopic region and at modest moisture content, i.e., film and hygroscopic correction models, which highlight need for further research. Also of interest, is how to address the situational difference between absorption, redistribution and drying of moisture when calculating the hydraulic conductivity for the full moisture range. The scientific novelty of the current study only addresses absorption.

Credit author statement

Jon Ivar Knarud: Conceptualization, Methodology, Validation, Formal analysis, Investigation, Writing - Original Draft, Visualization. **Tore Kvande:** Writing - Review & Editing, Supervision. **Stig Geving:** Writing - Review & Editing, Supervision.

Declaration of Competing Interest

The authors declare that they have no known competing financial interests or personal relationships that could have appeared to influence the work reported in this paper.

Acknowledgment

The authors gratefully acknowledge the financial support by The Research Council of Norway and several partners through the centre for Research-based Innovation "Klima 2050" (Grant No 237859) (www.klima2050.no).

Appendix A. Table A.1: Input applied to Eq. (42)

Table A.1
Coefficients for retention curves.

Material	w_{lim}	$n_{w,0}$	$l_{w,1}$	$l_{w,2}$	$l_{w,3}$	$l_{w,4}$	$c_{w,1}$	$c_{w,2}$	$c_{w,3}$	$c_{w,4}$	$n_{w,1}$	$n_{w,2}$	$n_{w,3}$	$n_{w,4}$
Brick Derluyn	1.0	0.4	0.846	0.154	0	0	1.40E-05	9.02E-06	–	–	4	1.69	–	–
Brick Carmeliet	0.7	1	0.054	0.455	0.491	0	3.84E-04	2.76E-05	1.72E-05	–	1.6	1.691	4.457	–
Brick Scheffler	1.7	0.65	0.02	0.21	0.65	0.12	3.7E-03	4.00E-05	6.72E-06	7.44E-07	1.6	5	4	4
Sand-lime brick Carmeliet	9.0	0.8	0.08	0.09	0.74	0.09	4.02E-05	9.99E-06	1.34E-06	9.49E-08	6	1.7	1.74	3.2
Sand-lime brick Scheffler	16	0.35	0.25	0.25	0.4	0.1	5.91E-06	1.51E-06	2.92E-07	4.83E-08	3	4	4.2	2.3
Calcium silicate Scheffler	3	2.5	0.63	0.09	0.27	0.01	3.08E-05	1.13E-06	7.83E-07	5.25E-07	1.71	7	6.6	4
Calcium silicate Häupl	8.4	0.2	0.72	0.1	0.177	0.003	3.79E-06	1.64E-06	6.13E-07	3.51E-08	5	8	3.5	8
Limestone	1	1	0.997	0.003	0	0	4.94E-05	5.00E-05	–	–	3.14	3.32	–	–
Aerated concrete	8	1.2	0.1	0.6	0.24	0.06	4.35E-05	6.85E-06	1.42E-06	9.90E-08	2	4	2	5
Cement mortar	16	0.55	0.35	0.07	0.58	0	2.25E-08	5.49E-08	2.81E-07	–	3.2	2.8	2.8	–
Concrete	25	0.45	0.2	0.8	0	0	3.32E-08	5.18E-08	–	–	3.4	2	–	–

Appendix B. Log(K)-log(pc) graphs of materials (Fig. 3 equivalent)

a) Brick (Derluyn)

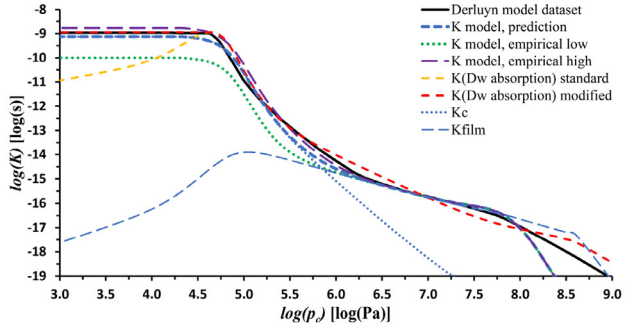

b) Brick (Carmeliet)

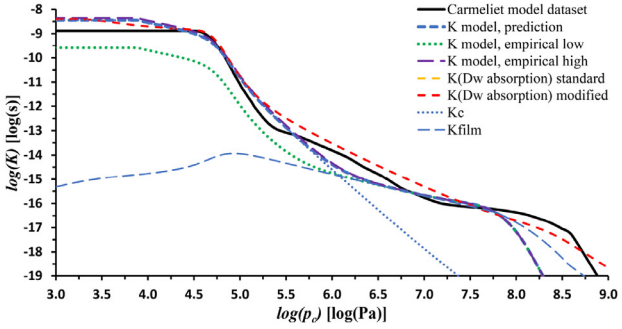

c) Brick (Scheffler)

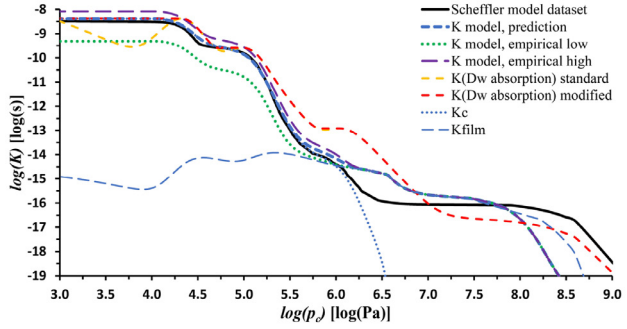

d) Sand-lime brick (Carmeliet)

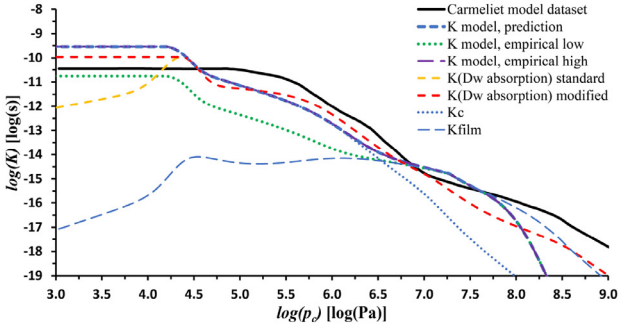

e) Sand-lime brick (Scheffler)

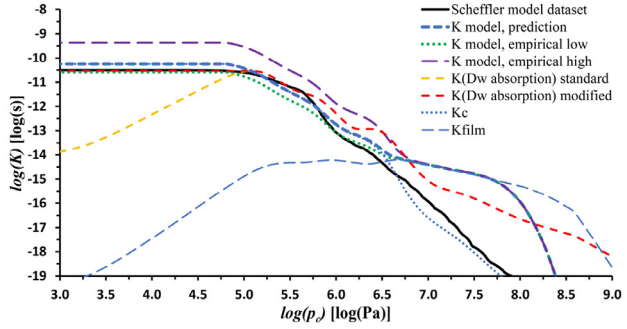

f) Calcium silicate (Scheffler)

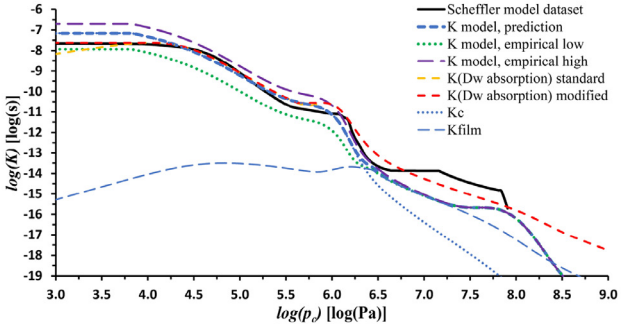

g) Calcium Silicate (Häupl)

h) Limestone

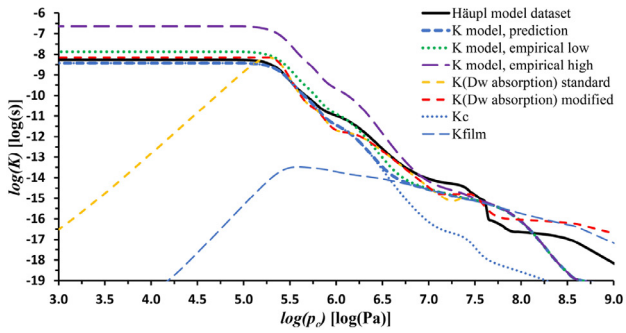

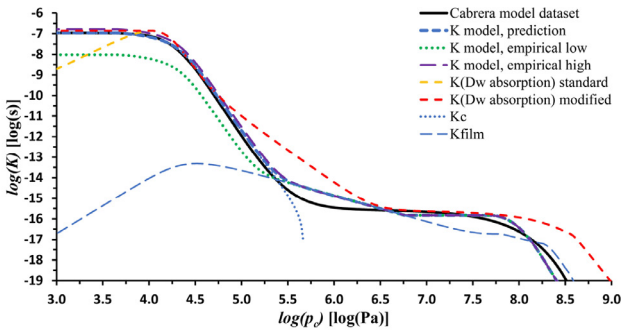

i) Aerated concrete

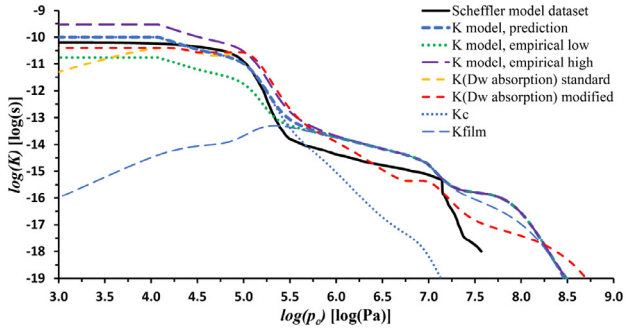

j) Cement mortar

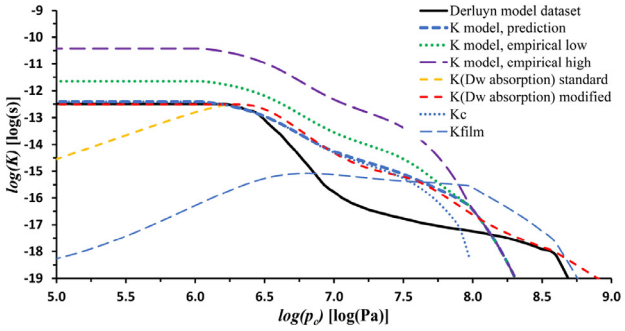

k) Concrete

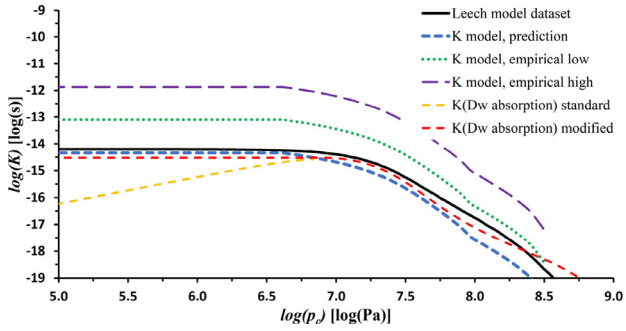

References

[1] J. Carmeliet, S. Roels, Determination of the isothermal moisture transport properties of porous building materials, J. Build. Phys. 24 (3) (2001) 183–210.

[2] F. Descamps, Continuum and Discrete Modelling of Isothermal Water and Air Transfer in Porous Media, Katholieke Universiteit Leuven, Leuven, Belgium, 1997.

[3] N.T. Burdine, in: Relative Permeability Calculations from Pore Size Distribution Data, 198, Petroleum Transactions, AIME, 1953, pp. 71–78.

[4] Y. Mualem, A new model for predicting the hydraulic conductivity of unsaturated porous media, Water Resour. Res. 12 (3) (1976) 513–522.

[5] M.T. Van Genuchten, A closed-form equation for predicting the hydraulic conductivity of unsaturated soils, Soil Sci. Soc. Am. J. 44 (5) (1980) 892–898.

[6] A.G. Hunt, R.P. Ewing, R. Horton, What's Wrong with Soil Physics? Soil Sci. Soc. Am. J. 77 (6) (2013) 1877–1887.

[7] G.A. Scheffler, R. Plagge, A whole range hygric material model: modelling liquid and vapour transport properties in porous media, Int. J. Heat Mass Transf. 53 (1) (2010) 286–296.

[8] W. Durner, Hydraulic conductivity estimation for soils with heterogeneous pore structure, Water Resour. Res. 30 (2) (1994) 211–223.

[9] W. Durner, Predicting the unsaturated hydraulic conductivity using multi–porosity water retention curves, Indirect Methods for Estimating the Hydraulic Properties of Unsaturated Soils (1992) 185–202.

[10] J. Grunewald, P. Häupl, M. Bomberg, Towards an engineering model of material characteristics for input to ham transport simulations - Part 1: an approach, J. Therm. Envelope Build. Sci. 26 (4) (2003) 343–366.

[11] M. Lebeau, J.-.M. Konrad, A new capillary and thin film flow model for predicting the hydraulic conductivity of unsaturated porous media, Water Resour. Res. 46 (12) (2010).

[12] A. Peters, Simple consistent models for water retention and hydraulic conductivity in the complete moisture range, Water Resour. Res. 49 (10) (2013) 6765–6780.

[13] J. Cai, E. Perfect, C.-.L. Cheng, X. Hu, Generalized modeling of spontaneous imbibition based on hagen–poiseuille flow in tortuous capillaries with variably shaped apertures, Langmuir 30 (18) (2014) 5142–5151.

[14] B. Ghanbarian, A.G. Hunt, R.P. Ewing, M. Sahimi, Tortuosity in porous media: a critical review, Soil Sci. Soc. Am. J. 77 (5) (2013) 1461–1477.

[15] M.S. Paterson, The equivalent channel model for permeability and resistivity in fluid-saturated rock—a re-appraisal, Mech. Mater. 2 (4) (1983) 345–352.

[16] A.C.M. Franken, J.A.M. Nolten, M.H.V. Mulder, D. Bargeman, C.A. Smolders, Wetting criteria for the applicability of membrane distillation, J. Memb. Sci. 33 (3) (1987) 315–328.

[17] H. Wong, S. Morris, C.J. Radke, Three-dimensional menisci in polygonal capillaries, J. Colloid Interface Sci. 148 (2) (1992) 317–336.

[18] G. Mason, N.R. Morrow, Meniscus curvatures in capillaries of uniform cross–section, J. Chem. Soc. Faraday Trans. 80 (9) (1984) 2375–2393 1: Physical Chemistry in Condensed Phases.

[19] G. Scheffler, Validation of Hygrothermal Material Modelling Under Consideration of the Hysteresis of Moisture Storage, Dresden University of Technology, Dresden, Germany, 2008.

[20] E.O. Macagno, Historico-critical review of dimensional analysis, J. Franklin Inst. 292 (6) (1971) 391–402.

[21] V. Beltran, A. Escardino, C. Feliu, M.D. Rodrigo, Liquid suction by porous ceramic materials, Brit. Ceramic Trans. J. 87 (2) (1988) 64–69.

[22] L.L. Handy, Determination of effective capillary pressures for porous media from imbibition data, Trans. AIME 219 (01) (1960) 75–80.

[23] I. Rodionova, E. Shkol'nikov, V. Volkov, The effect of fluid properties on the hydrodynamic permeability coefficient, Colloid J. (Kolloidnyi Zhurnal) 67 (4) (2005) 469–477.

[24] D. Benavente, P. Lock, M. Ángeles García Del Cura, S. Ordóñez, Predicting the capillary imbibition of porous rocks from microstructure, Transp. Porous Media 49 (1) (2002) 59–76.

[25] I. Ioannou, C. Hall, M.A. Wilson, W.D. Hoff, M.A. Carter, Direct measurement of the wetting front capillary pressure in a clay brick ceramic, J. Phys. D Appl. Phys. 36 (24) (2003) 3176–3182.
[26] M. Dejam, H. Hassanzadeh, Z. Chen, Reinfiltration through liquid bridges formed between two matrix blocks in fractured rocks, J. Hydrol. (Amst.) 519 (2014) 3520–3530.
[27] R. Sarfati, D.K. Schwartz, Temporally Anticorrelated Subdiffusion in water Nanofilms on silica suggests near-surface viscoelasticity, ACS Nano 14 (3) (2020) 3041–3047.
[28] EN ISO 12572, Hygrothermal Performance of Building Materials and Products - Determination of Water Vapour Transmission Properties, European Committee for Standardization (CEN), Brussels, Belgium, 2001.
[29] C.-.E. Hagentoft, HAMSTAD, Final report: Methodology of HAM-modeling, Report R-02, Chalmers University of Technology, Gothenburg, Sweden, 2002.
[30] N. Lu, Generalized soil water retention equation for adsorption and capillarity, J. Geotech. Geoenviron. Eng. 142 (10) (2016) 04016051.
[31] J. Carmeliet, S. Roels, Determination of the moisture capacity of porous building materials, J. Therm. Envelope Build. Sci. 25 (3) (2002) 209–237.
[32] A. Revil, N. Lu, Unified water isotherms for clayey porous materials, Water Resour. Res. 49 (9) (2013) 5685–5699.
[33] H. Derluyn, P. Moonen, J. Carmeliet, Moisture transfer across the interface between brick and mortar joint, in: Proceedings of the 8th symposium on building physics in the nordic countries, Technical University of Denmark, Copenhagen, Denmark, 2008, pp. 865–872.
[34] P. Häupl, H. Fechner, H. Petzold, Interior retrofit of masonry wall to reduce energy and eliminate moisture damage: comparison of modeling and field performance, Thermal Performance of Exterior Envelopes of Whole Buildings IX: International Conference, ASHRAE, 2004.
[35] V. Cabrera, R. López-Vizcaíno, Á. Yustres, M.Á. Ruiz, E. Torrero, V. Navarro, A functional structure for state functions of moisture transfer in heritage building elements, J. Build. Eng. 29 (2020) 101201.
[36] C.A. Leech, Water Movement in Unsaturated Concrete, The University of Queensland, Brisbane, Qld, Australia, 2003.
[37] C. Leech, D. Lockington, R.D. Hooton, G. Galloway, G. Cowin, P. Dux, Validation of Mualem's conductivity model and prediction of saturated permeability from Sorptivity, ACI Mater. J. 105 (1) (2008) 44–51.
[38] Y. Bo-Ming, L. Jian-Hua, A geometry model for tortuosity of flow path in porous media, Chin. Phys. Lett. 21 (8) (2004) 1569–1571.
[39] M. Raimondo, M. Dondi, D. Gardini, G. Guarini, F. Mazzanti, Predicting the initial rate of water absorption in clay bricks, Constr. Build. Mater. 23 (7) (2009) 2623–2630.
[40] A. Merioua, A. Bezzar, F. Ghomari, Non-destructive electrical methods for measuring the physical characteristics of porous materials, J. Nondestr. Eval. 34 (2) (2015) 1–12.
[41] H. Garbalińska, M. Stasiak, M. Bochenek, G. Musielak, Assessment of a new method for determining the relationship between effective diffusivity and moisture concentration – exemplified by autoclaved aerated concrete of four density classes, Int. J. Heat Mass Transf. 124 (2018) 288–297.
[42] G.M. Laudone, C.M. Gribble, K.L. Jones, H.J. Collier, G.P. Matthews, Validated a priori calculation of tortuosity in porous materials including sandstone and limestone, Chem. Eng. Sci. 131 (2015) 109–117.
[43] J. Carmeliet, H. Hens, S. Roels, O. Adan, H. Brocken, R. Cerny, Z. Pavlik, C. Hall, K. Kumaran, L. Pel, Determination of the liquid water diffusivity from transient moisture transfer experiments, J. Therm. Envelope Build. Sci. 27 (4) (2004) 277–305.
[44] C.R. Pedersen, Combined Heat and Moisture Transfer in Building Constructions, Technical University of Denmark, Lyngby, Denmark, 1990.
[45] H.M. Künzel, Simultaneous Heat and Moisture Transport in Building Components, Fraunhofer IRB-Verlag, Stuttgart, Germany, 1995.
[46] D. Lockington, J.Y. Parlange, P. Dux, Sorptivity and the estimation of water penetration into unsaturated concrete, Mater. Struct. 32 (5) (1999) 342.
[47] J. Carmeliet, H. Janssen, H. Derluyn, An improved moisture diffusivity model for porous building materials, in: Proceedings of 12th Symposium for Building Physics, Dresden, Germany, 2007.
[48] M. Krus, Moisture Transport and Storage Coefficients of Porous Mineral Building Materials: Theoretical Principles and New Test Methods, Fraunhofer IRB Verlag, Stuttgart, Germany, 1996.
[49] R.W. Vervoort, S.R. Cattle, Linking hydraulic conductivity and tortuosity parameters to pore space geometry and pore-size distribution, J. Hydrol. (Amst.) 272 (1) (2003) 36–49.
[50] V.I. Nikitsin, B. Backiel-Brzozowska, Determining hydraulic radii of construction wall materials in capillary moisture transfer, Int. J. Heat Mass Transf. 88 (2015) 558–564.